Magnus Dale Johnsen

Study of laminar and turbulent flow in a square cross-section prepared for PIV measurements

Master's thesis in Mechanical Engineering
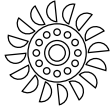Supervisor: Chirag Trivedi
June 2022

NTNU
Norwegian University of
Science and Technology

Magnus Dale Johnsen

Study of laminar and turbulent flow in a square cross-section prepared for PIV measurements

NTNU
Norwegian University of
Science and Technology

Waterpower Laboratory

NTNU

Abstract

Hydropower, in form of efficient turbines with long-life expectancy, is expected to play a key role in the green transition. An understanding of fundamental fluid mechanics is essential for this. The utilization of experimental data in form of particle image velocimetry (PIV) is a leading method for achieving this insight. In this regard, NTNU's Waterpower Laboratory is aiming to build a state-of-the-art PIV test facility for production of accurate data and education. To ensure high-quality flow characteristics in the test area, all elements of the experimental facility are customized. A computational fluid dynamic investigation of the pressurized tank was completed in this thesis for four different designs, including a base case, to determine which one produces the most optimal flow field for the pump and test section. The key difference between the configurations was flow conditioners used in different combinations. All the flow conditioners in the simulations were modeled using the porous domain approach. Each configuration was subjected to transient simulations using $k - \omega$ SST model in ANSYS® CFX®.

All configurations showed significant improvement. In comparison to the base scenario, each combination contributed to a calmer and uniform flow in the tank. A thin flow conditioner, followed by a thick one, yielded the most promising results. This combination had a pronounced ability to reduced the vorticity in the tank as well. One simulation was also conducted with this configuration for the entire system. Despite slight variations in tank results, the setup resulted in high-quality flow characteristics in the test area. As a result, this thesis recommends that the design consisting of one thin and one thick flow conditioner be used. This will enable suitable flow characteristics in the test section for the optical measurements of different engineering structures, including, bluff body, cylinder, hydrofoil, blade profile, convergent, divergent sections, etc.
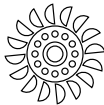
Sammendrag

Vannkraft, i form av effektive turbiner med lang levetid, forventes å spille en nøkkelrolle i den grønne omstillingen. En forståelse av grunnleggende fluidmekanikk er avgjørende for dette. Utnyttelsen av eksperimentelle data i form av partikkelbildehastighetsmåling (PIV) er en ledende metode for å oppnå denne innsikten. I denne forbindelse har NTNU's vannkraftlaboratorium som mål å bygge et topp moderne PIV-testanlegg for produksjon av nøyaktige data og til utdanning. For å sikre høykvalitets strømningsegenskaper i testområdet, tilpasses alle segmentene i forsøksanlegget. En numerisk fluidynamisk (CFD) undersøkelse av trykktanken ble utført i denne oppgaven for fire forskjellige design, inkludert et kontrolltilfelle, for å undersøke hvilken som produserer det mest optimale strømningsfeltet for pumpen og testseksjonen. Den viktigste forskjellen mellom konfigurasjonene var strømingsrettere brukt i forskjellige kombinasjoner. Alle strømningsretterene i simuleringene ble simulert ved bruk av den porøse domene tilnærmingen. Hver konfigurasjon ble simulert ved å bruke $k - \omega$ SST-modellen.

Alle konfigurasjoner viste en betydelig forbedring. Sammenlignet med kontroll tilfelle bidro hver kombinasjon til en mer rolig og jevn flyt i tanken. En tynn strømingsretter, etterfulgt av en lang, ga de mest lovende resultatene. Denne kombinasjonen hadde en utpreget evne til å redusere virvlene i tanken. En simulering ble også utført med denne konfigurasjonen for hele systemet. Til tross for små variasjoner i tankresultater, resulterte oppsettet i høykvalitets strømningsegenskaper i testområdet. Som et resultat av dette anbefaler oppgaven at det benyttes et design som består av en tynn og en lang strømningsretter.

Acknowledgments

Contents

List of tables

x

List of figures

xiii

Nomenclature

Abbreviation

CFD   Computational fluid dynamic

NS   Navier-Stokes equation

NTNU Norwegian University of Science and Technology

PIV   Particle image velocimetry

RANS Reynolds-averaged Navier-Stokes equation

SST   Shear stress transport

TKE   Turbulent kinetic energy

Latin symbols

A Cross section area

D Diameter (m)

f Body forces

h Height (m)

k Turbulent kinetic energy ($\mathrm{m^2\ s^{-2}}$)

L Characteristic length

l Thickness (m)

N Number of elements

P	Average pressure (Pa)
p	Pressure (Pa)
p'	Fluctuating pressure (Pa)
Q	Mass flow
t	Time (s)
U	Average velocity (m s^{-1})
u	Velocity (m s^{-1})
u'	Fluctuating velocity (m s^{-1})
V	Uniformity

Dimensionless numbers

Re	Reynolds number
TI	Turbulent Intensity

Greek symbols

ϵ	Rate of dissipation of turbulent kinetic energy (m^2 s^{-3})
ν	Kinematic viscosity (Pa s)
ν_t	Eddy viscosity (Pa s)
ω	Specific dissipation
ρ	Density (m^2 s^{-1})

Superscripts and subscripts

a	Average
e	Effective
i, j	Indices
T	Transverse
S	Streamwise

————————————— Chapter 1—————————————

Introduction

1.1 Background

The electricity demand is predicted to increase in the forthcoming decades. Combining this with that almost 75% of the electricity today comes from non-renewable sources means that the greenhouse gas emissions will keep increasing unless a transition to renewable energy sources occurs [3]. Hydropower is a clean, reliable and environment friendly source of energy. It produces approximately 16% of all the electricity in the world and is by far the largest renewable source (2019) [3]. Compared to other renewable energy sources, hydropower has the advantage to easily store energy in form of reservoir, making it possible to produce energy when the demand is high.

Renewable energy sources covered about 97% of the electric energy consumption in Norway in 2018 [4]. Amongst this, 88% comes from hydropower. Norway has therefore a highly intensive to improving hydropower plants, both when it comes to efficiency and to prolonged life expectancy. To be able to do this, it is important to have a thorough understand of how flow behaves. This understanding can be attained with the help of research, study, computational fluid dynamics (CFD) and experimental fluid dynamics.

Experiments have had a leading role in developing hydropower technology. This is something the Waterpower Laboratory at NTNU is acknowledging and is therefore in the planning and designing phase of obtaining a dedicated experimental rig to use for particle image velocimetry (PIV).

PIV is one of the most prominent ways to measure velocity profile today. The method consists of inserts small, non-buoyant and reflective particles into a flow. A flow section is then illuminated with a laser creating reflections captured by a high-resolution camera. By comparing two images, a velocity

vector field can be extracted.

These experiments give an important insight in fundamental fluid dynamics, but have quite specific demands for the flow characteristics in the test section to be able to produce high quality results. The design of the test setup is therefore of the upmost importance and has to be customized for different types of experiments.

One normal experimental setup for PIV is a closed-circuit water tunnel. Water tunnels can be used as a multipurpose facility. The primary utilization are experiments, but it can also be utilized to calibration as well as education and training. The design of a water tunnel is therefore centered around the test section. There are many segments that affect the flow in different way that often are used to produce a desirable environment, including diffuser, converger and tanks.

A powerful tool in the design phase of a water tunnel is the use of CFD. It provides a way to test and confirm the systems performance at an early stage. This confirmation can provide areas of improvement and potentially save both valuable time and cost. This thesis will focus on doing CFD analysis on the flow through the storage tank that are a part of the water tunnel.

Tanks have been in use within experimental fluid dynamics for a long time. It is used for pressure control, to slow down or control the flow and for housing for necessary equipment. Flow entering a storage tank undergoes a rapid expansion that can cause severe turbulence and disturbances in from of swirls and vortexes. These disturbances in the flow can propagate through system. In a test rig for experimental PIV, this can alter the quality and accuracy of the results. It is therefore important to design a loop that get rid itself of the larges disturbances and deliver a steady flow profile in the test section.

1.2   The objective

The goal of this thesis is to investigate the effect of and recommend a combination of thin and thick flow conditioners to use in the tank of the state-of-the-art experimental facility for PIV. The facility is intended for producing highly accurate data as well as education of students. The investigation consisting of CFD-analysis on pre-selected configuration. There are selected a total of four configurations to investigate, including the base case. This
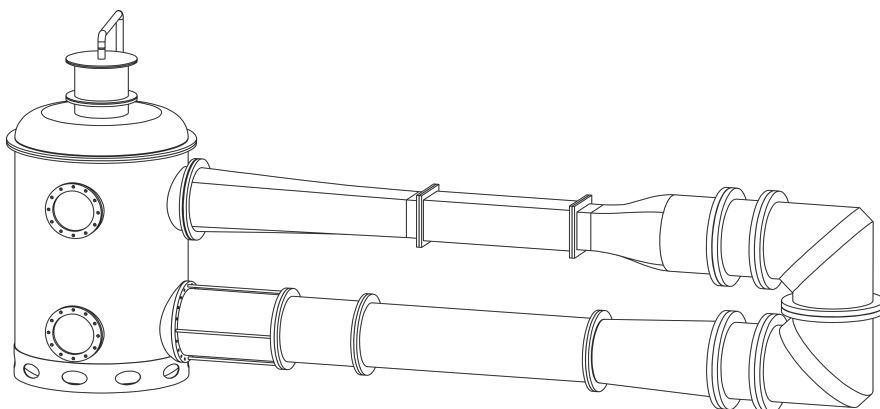
Figure 1.1: Provisional sketch of the test setup for PIV measurements in the Waterpower Laboratory.

thesis shall also be the groundwork for the further development of the state-of-the-art experimental setup for optical measurements, such as PIV, LDV, etc.

1.3 Limitations

Even though CFD is primary used to save time compared to experiments, it can be a time consuming and costly activity. This means that even though the setup time is time saving, the entire process takes time. This comes in effect when deciding how many simulations to run and what settings to use. The result is some reduction in what simulations to run based on what kind of information they can return.

Complex geometry is also a big limitation for CFD. There are therefore a standard to simplify geometry in regions with reduced effort. It is also acceptable to simplify geometry in regions where there will be challenging to create high quality mesh. Based on this, some simplifications have been done on the geometry. These simplifications will be described in more detail in the Section 3.3. The adopted simplifications did not alter the flow field significantly. Main objective of the present work was preserved fairly well.

———————————Chapter 2———————————

Literature review

This chapter will give an overview on what work that has already been done within relevant topics. It will focus on the elements that are important when designing a water tunnel and how each one affects the flow. It also described elements important when deciding which pump to implement in the configuration.

Despite experimental setups being used for a long time, there is no normalized method to create a good environment for experimental testing. Instead, there are some principal component that are present in almost all setups to help achieve optimal flow conditions [5] . The flowchart shown in Fig. 2.1 is a simplified visualization of how to design a water tunnel. The entire circuit is designed around the targeted velocity and Reynolds number in the test section [1]. The rest of the sections are adjusted to fulfill the criteria for the flow in the test sections as seen in the leftmost box.

These are the components used in the design of this water tunnel. Some of them may have been used more than once:

- Test section
- Diffuser
- Thin flow conditioner
- Multipurpose tank
- Thick flow conditioner
- Converger
- Elbow
- Pump
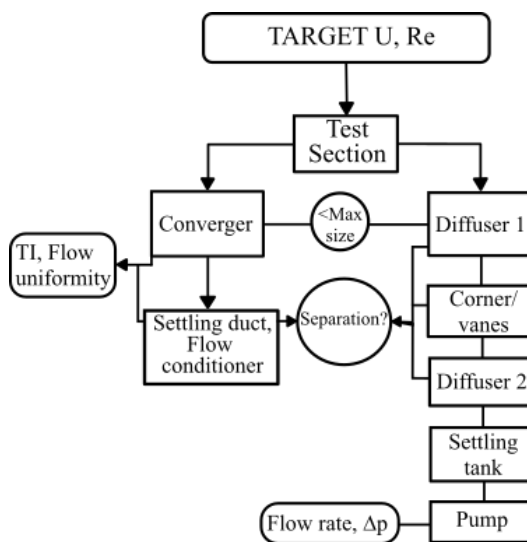
Figure 2.1: A simplified flowchart of how to design a water tunnel with focus on the different components that are a part of the system [1].

Test section

The test section is designed based on the experiments planned to be conducted. This includes size to achieve desirable Reynolds number as well as cross section area to have a low blocking factor [5]. To produce high quality results at an experimental rig, it is important that the flow in the test section fulfills certain criteria such as uniform flow, devoid of unintended unsteadiness and secondary flow and low turbulent intensity (TI) [1].

Converger and diffuser

When a flow enters a converger, the cross section decreases forcing the flow to accelerate. This causes pre-existing vortex filaments to stretch, resulting in reduction in lateral fluctuation and lower TI [6]. This statement is backed by numerical and experimental data [7, 8]. The boundary layer is also reset, creating a more uniform velocity profile at the outlet of the converger [6].

The diffusers task is to decelerate the flow and regain pressure while minimizing loss [9]. A shorter diffuser with a equivalent cone angle of around

$10°$ gives the best pressure recovery [10]. A high angle on the other hand makes a flow more unsteady and prone for separation. Some suggest that the best cone angle for flow steadiness is around $5°$ [10]. Others concludes that the cone angle should not exceed $3.5°$, resulting in a longer segment [11].

Elbow

A flow in a closed circuit is bound to undergo corners which can be a source of disturbance in a flow. It makes the flow prone to separation and secondary flow illustrated in Fig. 2.2 [2, 12]. In an attempt to reduce or delay the separation, guide vanes are often introduced to the bend [13]. The guide vanes curve the flow and align the streamlines at the outlet of the bend. The presence of secondary flow patterns are also much weaker [13]. By introducing guide vanes, the flow after the bend is therefore more uniform flow. A result of the bend disturbing the flow is an additional pressure loss over the bend [12]. The pressure loss is often presented as a pressure loss coefficient, K [14]. There are some contradictions in what the true values of K are and which parameters affecting it. Despite this, there is a consensus that guide vanes help reduce the pressure loss.
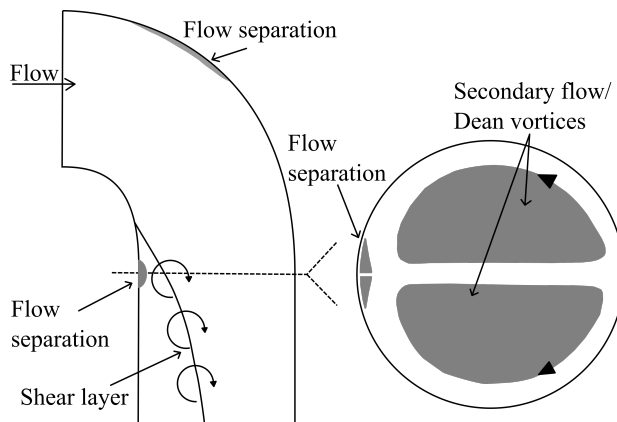
Figure 2.2: Effects of flow undergoing a sharp turn [2].

Thin and thick flow conditioners

Based on the ISO-5167 standard, upstream disturbances such as a bend can require a length up to 100D to recover to fully developed velocity profile

[15]. In most situations, there is a size criterion making it impossible to fulfill such a design.

Extensive research has therefore been conducted of thin and thick flow conditioners to achieve fully developed flow and swirl-free flow in shorter distances. It has also been a goal to standardize the flow.

Thin flow conditioner have many parameters such as porosity, number of holes and design, which all affect the performance. Perforated plates with equally sized holes are a widespread design [16, 17]. Studies comparing different porosities (45%-70%) shows that they can produce axial velocity profile within the ISO-standard in a few diameters length [18]. A great reduction from letting the flow stabilize itself.

Another effect that depends highly on the parameters is the turbulent kinetic energy (TKE) [18]. Plates with high porosity creates profile with much lower TKE in the wake then for plates with low porosity. This increase in TKE will speed up the mixing in the flow. For flows with close to uniform velocity fields upstream from the thin flow conditioner this will result in an increase in length to reach fully developed, where the TKE is normally lower. On the other hand, for a case with more chaotic flow fields upstream, this mixing can tribute to a faster development.

Thick flow conditioners have the same properties as the thin ones, but with a much larger thickness. They will therefore affect the flow in a similar manner. In addition to this, the flow conditioner has the effect of streamlining the flow, minimizing secondary flow.

Porous media

The porous media approach has been more and more widespread. It is a method that simplifies porous domains and models the volume in question instead of solving it. This method is often used for heat exchangers, flow conditioners and other complex porous geometries [19, 20].

Studies comparing experimental velocity and pressure fields behind a perforated plate to two CFD simulations showed that the porous media approach yielded an error an average error of 6% on the velocity field [21]. The pressure field on the other hand had considerably higher errors.

Tank

Several studies have been conducted to get a better understanding of how flow in large storage tanks behaves. Many of these studies has focused on aspects outside the scope of this thesis but in the process gain knowledge translatable to this case. CFD studies of flow in tanks reveals information on the velocity. Velocity fields with pairs of vortecies are easily recognized [22]. Some of the vortecies were directly coupled to be effect of buoyancy, yet some of the vortices were distinct coupled to the inlet and geometry [23].

These vortices are a consequence of mainly two aspects. The first one is the inlet flow enters the tank with high velocity and hitting the back wall and splitting into two flows along the back wall. This will create large vortices in the flow. Since a normal feature of tank geometry is symmetry, the vortex flow will be symmetrical as well.

The second aspect that creates vortices are the rapid expansion the flow undergoes when entering the tank. These vortices are not as large length scale as the other, but does have an effect on the flow [24].

Pump

Axial flow pumps are designed to be the drive force for a flow. Ideally, the flow into the pump should be uniform, steady, and free from swirl. Much like the flow in the test section. Any lack of uniformity through inlet connection can result in pumps not operating to optimum design condition and at a lower hydraulic efficiency [25].

Several studies where vortex generators (VG) have been placed in front of a axial flow pump has been conducted to investigate how pre-existing vortexes influences the efficiency and performance of the impeller. The conclusion states a clear connection between the uniformity and efficiency [26, 27].

The phenomenon of an inflow vortex can sometimes cause an increase in pressure fluctuation and cavitation. This can lead to instability in the pump operation. Phenomenons including intense vibration, large noise and serious efficiency reductions can occur [26]. The literature also makes the point that asymmetry is undesirable. With a reduced number of blades, the pressure pulsation of the fluid in the pump becomes stronger and enhanced the vibration induced by the flow [28].

From the project thesis, the design velocity and Reynolds number was tested and a range was decided. These flow rates are achieved by installing a

pump with the right pump characteristics. The overall task for the pump is to move flow from the tank into the circuit towards the test section. To run experiments at different Reynolds's number, the application range is wanted to be broad. The pump also needs to be able to support the head equal to the pressure loss through the entire circuit. Due to the customized tunnel, there is no empirical data on the pressure loss so it is estimated by the use of Darcy's friction equation and pressure loss coefficients for the specialized parts.

Alongside this, there are all the technical aspects such as how to implement the pump into the tank. The challenge of the tank being the housing for the pump is the assemble. By creating support by the floor or roof of the tank, there are much equipment that will tribute to disturbing the flow. The best way to connect the pump is through the shroud and the wall of the tank.

—————————Chapter 3—————————

Theory and methods

The theory and methods chapter is here to create a clear understanding of which approach and methods have been used to achieve the results presented in the result chapter. This chapter will first present the relevant theory used in the solution approach and important aspects of the post-processing. After the theory is presented, the geometry used in the simulation will be introduced and defined. The mesh and simulation settings including boundary conditions will be described towards the end of the chapter.

3.1 Governing equations

The governing equation for fluid motion is based on the conservation of physical quantities. Conservation of mass is described in the continuity equation, whereas conservation of momentum is known as the Navier-Stokes equation (NS). For an incompressible flow where the density, ρ, and the kinematic viscosity, ν, is considered constants, the Navier-Stokes can be written as

$$\frac{\partial u_i}{\partial t} + u_j \frac{\partial u_i}{\partial x_j} = -\frac{1}{\rho}\frac{\partial p}{\partial x_i} + \nu \frac{\partial^2 u_i}{\partial x_j \partial x_j} + f_i \qquad (3.1)$$

where u is the instantaneous velocity vector, x is the spatial coordinates vector in Cartesian coordinates and f_i is the body forces.

Most of the flows that is encountered every day is turbulent. Turbulence is a 3-dimensional time dependent phenomenon and is often characterized by apparently random and chaotic instantaneous motion. These motions

happens on all length scales in a flow, from the characteristic length of the geometry to the smallest scales where energy dissipates to heat. Turbulence occurs at relative high Reynolds numbers, Re. The Reynolds number is a nondenominational value defined as the ratio between inertial forces and viscous force and is defined like this

$$Re = \frac{UL}{\nu} \tag{3.2}$$

where U is the characteristic velocity and L is the characteristic length. For flow in a pipe the characteristic length is the hydraulic diameter and the flow is considered turbulent when $Re > 2500$.

As mentioned, a turbulent velocity profile is highly time dependent. The velocity and pressure can therefore be decomposed into time dependent and independent components.

$$u_i = U_i + u_i' \qquad p_i = P_i + p_i' \tag{3.3}$$

where U represent the average velocity, P is the average pressure and, u' and p' is the time dependent fluctuation for velocity and pressure respectively. The turbulent intensity can now be defined as

$$TI = \frac{u'}{U} \tag{3.4}$$

and describes the fluctuating relative to the velocity magnitude.

By inserting Eq. 3.3 into Eq. 3.1 and averaging the equation the Reynolds Average Navier-Stokes (RANS) equation is derived

$$\frac{\partial U_i}{\partial t} + U_j \frac{\partial U_i}{\partial x_j} = -\frac{1}{\rho} \frac{\partial P}{\partial x_i} + \nu \frac{\partial^2 U_i}{\partial x_j \partial x_j} - \frac{\partial (\overline{u_i' u_j'})}{\partial x_j} + F_i, \tag{3.5}$$

where F is the average body forces. The term, $\overline{u_i' u_j'}$ in Eq. 3.5, is known as the Reynolds stresses. Combining it with the a factor of $\frac{1}{2}$ the TKE is obtained

$$k = \frac{1}{2} \overline{u_i' u_i'}. \tag{3.6}$$

12

Vortex

Vortexes region in a fluid in which the flow revolves around in an axis line. This axis can either stand still or move together with the bulk flow. Vortexes is a major component when talking about turbulent flow and comes in all sizes, from smallest length scale to the length scale of the entire system. They can be generated several different ways and can have a greatly impact on the flows nature. The mathematical formula of vertices is the curl of the flow and is denoted as

$$\vec{\omega} = \nabla \times \vec{u} \tag{3.7}$$

where $\vec{u}$ is the velocity vector and ∇ is the nabla operator. The magnitude of the vorticity gives information of the rotating motion. The orientation of the vorticity is decided by use of the right-hand rule. Positive value translates into counterclockwise rotation.

Uniformity

The uniformity of an axial velocity distribution is often calculated by

$$\overline{V}_a = \left[1 - \frac{1}{\overline{v}_a} \sqrt{\frac{\sum_{i=1}^{n} (v_i - \overline{v}_a)^2}{n}} \right] \times 100\% \tag{3.8}$$

$$\overline{v}_a = \frac{Q}{A} \tag{3.9}$$

where $\overline{V}_a$ is the uniformity, Q is the mass flow and A is the area of the calculation plane. v_i is the axial velocity for each calculation point and n is the total number of units. The closer $\overline{V}_a$ to 100% the more uniform the flow is.

Turbulence model

Neither Navier-Stokes nor RANS has an exact analytical solution. The fluid domain is therefore discretesized and solved numerically. The most used simulation approach is the RANS models. They solve the RANS equation and models the smallest scales. The RANS model approach provides

information about the average properties in the flow, which often is enough information to get a understanding of the flow.

Menter's SST is a blending combination of the well tested and acknowledged $k - \epsilon$ and $k - \omega$ model [29]. It utilizes the strength of $k - \omega$ ability to predict separation and wall bounded flow and $k - \epsilon$'s reliability in free-shear flows with small pressure gradients and recirculating flow. The $k - \omega$ SST model used in ANSYS® CFX® is defines as:

$$\frac{\partial(k)}{\partial t} + \frac{\partial(kU_j)}{\partial x_j} = \frac{\partial}{\partial x_j}\left[\left(\nu + \frac{\nu_t}{\sigma_{k3}}\right)\frac{\partial k}{\partial x_j}\right] + P_k - \beta' k\omega + P_{kb} \qquad (3.10)$$

and

$$\frac{\partial(\omega)}{\partial t} + \frac{\partial(U_j\omega)}{\partial x_j} = \frac{\partial}{\partial x_j}\left[\left(\nu + \frac{\nu_t}{\sigma_{k3}}\right)\frac{\partial \omega}{\partial x_j}\right]+$$

$$(1 - F_1)2\frac{1}{\sigma_{\omega 2}\omega}\frac{\partial k}{\partial k_j}\frac{\omega}{\partial x_j} + \alpha_3\frac{\omega}{k}P_k - \beta_3\omega^2 + P_{\omega b} \quad (3.11)$$

where β', σ_{k3}, σ_{k2}, α_3, β_3 are empirical found constants [30]. F_1 is a blending function and decides that slides SST between k - ω and k - ϵ. ν_t is the eddy viscosity. The F_1 and the eddy viscosity is defined as:

$$\nu_t = \frac{a_1 k}{max(a_1\omega, SF_2)}, \qquad (3.12)$$

$$F_1 = tanh(arg_1^4), \qquad (3.13)$$

$$arg_1 = \left(min\left(max\left(\frac{k}{\beta'\omega y}, \frac{500\nu}{y^2\omega}\right), \frac{4\rho k}{CD_{kw}\sigma_{\omega 2}y^2}\right)\right) \qquad (3.14)$$

S is an invariant measure of the strain rate and F_2 is another blending function.

$$F_2 = \tanh arg_2^2, \qquad arg_2 = \max\left[\frac{2\sqrt{k}}{0.09\omega y}, \frac{500\mu}{\rho y^2\omega}\right] \qquad (3.15)$$

where y is the distance to the nearest wall and

$$CD_{k\omega} = max\Big(2\rho \frac{1}{\sigma_{\omega 2}} \frac{\partial k}{\partial x_j} \frac{\partial \omega}{x_j}, 10^{-10}\Big). \tag{3.16}$$

When introducing a porous domain and chooses true velocity as setting, the governing equations are modified slightly and is now calculated as:

$$\frac{\partial}{\partial t}(\gamma\rho) + \nabla \cdot (\rho\mathbf{K} \cdot \mathbf{U}) = 0 \tag{3.17}$$

$$\frac{\partial}{\partial t}(\gamma\rho\mathbf{U}) + \nabla(\rho(\mathbf{K} \cdot \mathbf{U}) \times \mathbf{U}) - \nabla \cdot (\mu_e \mathbf{K} \cdot (\nabla\mathbf{U} + (\nabla\mathbf{U})^T - \frac{2}{3}\delta\nabla \cdot \mathbf{U}))$$
$$= \gamma\mathbf{S}_M - \gamma\nabla p \quad (3.18)$$

where γ is the volume porosity, μ_e is the effective viscosity and S_M is an added source term for momentum loss. S_M is defined in each direction as such:

$$\mathbf{S}_{M,x} = -\frac{\mu}{K_{perm}^S}U_x - K_{loss}^S \frac{\rho}{2}|\mathbf{U}|U_x \tag{3.19}$$

$$\mathbf{S}_{M,y} = -\frac{\mu}{K_{perm}^T}U_y - K_{loss}^T \frac{\rho}{2}|\mathbf{U}|U_y \tag{3.20}$$

$$\mathbf{S}_{M,z} = -\frac{\mu}{K_{perm}^T}U_z - K_{loss}^T \frac{\rho}{2}|\mathbf{U}|U_z \tag{3.21}$$

K_{perm}^S and K_{perm}^T is the streamwise and transverse permeabilities and K_{loss}^S and K_{loss}^T are the streamwise and transverse loss coefficients [31]. These can also be expressed as linear and quadratic resistance coefficients.

3.2 Numerical setup

CFD simulation is an alternative to experiments and shows great value for complex geometries or expensive setup and have the possibility to extract information that may prove difficult to extract in physical experiments.

CFD simulations can be divided in three main stages: pre-processing, simulation, and post-processing. The pre-processing stage consists of defining the geometry, mesh and boundary conditions. The simulation stage consists of using the constructed model for running simulations. In the post-processing stage the obtained result is analysed. This chapter will go through the stages in this order.

Geometry

The entire water tunnel is shown in Fig. 3.1. The geometry used in this thesis is reduced due to geometry out of scope and simulation time. The geometry used in the simulations is shown in Fig. 3.2. The flow inlet is placed at the square test section with dimensions 300 mm by 300 mm. From here the test section transforms into a circular pipe with a diameter of D_1 = 250 mm. The flow then passes a thin flow conditioner with thickness of l_1 = 7 mm and porosity of 80% before entering the tank. The tank itself has a diameter of D_2 = 1300 mm and a height h = 2524 mm. The flow exits the tank through a Amaline C5033-483/64URG axial impeller pump to the outlet pipe with diameter D_1 = 250 mm.
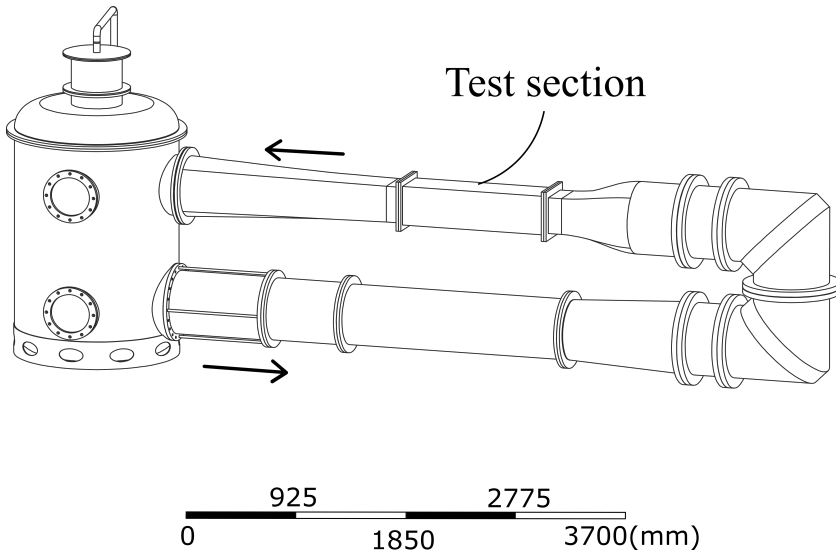
Figure 3.1: Complete geometry of water tunnel. The arrows indicate the flow direction.

16

The geometry to analyze consists of a cylindrical water storage tank. The inlet is a horizontal circular pipe at the upper half on the tank, whereas outlet is placed on the lower half. They are placed right on top of each other. A pump mounted at the inside of the tank at the outlet and is the driving force of the flow.
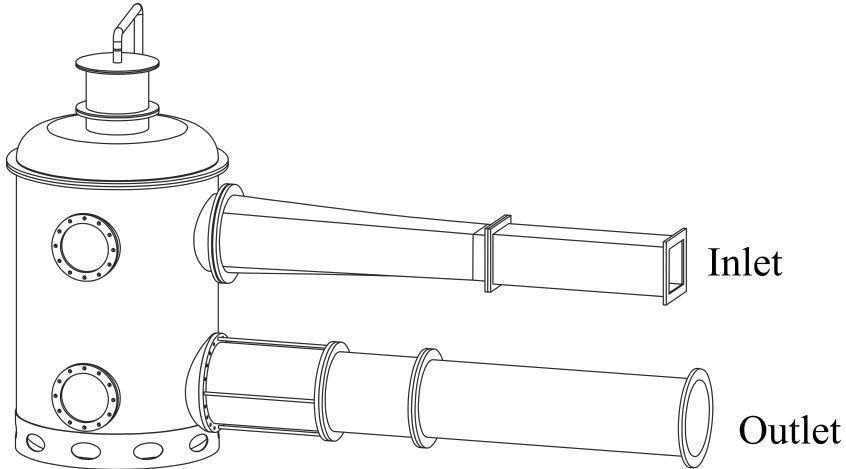
Figure 3.2: Components of water tunnel used in this thesis.

The tank geometry was pre-defined by an in-house designer at the Waterpower Laboratory whereas the pump geometry was provided by the producer and manufacturer of the pump. To assure that the geometry model given by the manufacturer was accurate, some of the key measurements on the pump were measured and compared. The key values can be found in Tab. 3.1. The relative errors are based on the physical model.

The errors are generally low and can be explained by the layer of paint that has been added to the pump to protect it from corrosion among other things. The biggest difference from the model and the physical part is the blades. Only one value has been shown here due to the large errors. The error is closer to 70% showing that the model is not accurate. During the measurements, it was also discovered that the blade geometry are mirrored compared to the model. Meaning that the trailing edge and leading edge has switched places. The result is being that the rotor will rotate the opposite direction direction. Since the rest of the simplified geometry is symmetric in the relevant axis's, these differences will not affect the simulations and the areas of interest will go unchanged.

17

Table 3.1: Key measurements taken from the physical pump.

Place/Value	Measures [mm]	Model [mm]	Relative error
Front cylinder	260.6	259	+0.6%
Back cylinder	259.9	258	+0.7%
Half cylinder height	29.6	29.5	+0.3%
Half cylinder length	172	170	+1.1%
Groove back depth	23	25	-8.7%
Groove back length	30.7	30.5	+0.7%
Groove front depth	50.8	51.5	-1.4%
Groove front length	18.2	18.5	-1.6%
Blade halfway leading edge	5.95	1.8	+69.7%

In addition to the tank and the pump, there are added flow conditioners in the tank in three different combinations. These are from here on out referred to as configurations. In addition to these three, there is a configurations where there is nothing additional added. That makes a total of four configurations that will be tested. The thin and thick flow conditioners are added to investigate which configuration provides the most desirable flow field through the tank, pump and lays the best foundation for the rest of the circuit. The flow conditioners are placed in two locations shown in Fig. 3.3.

Table 3.2: All configuration and their distinctions.

Configuration	Thin flow conditioner (A)	Thin flow conditioner (B)	Thick flow conditioner (B)
1	✓	✓	
2	✓		✓
3	✓		
4			

The different configurations and their distinctions can be seen in Tab. 3.2. The letter in the parenthesis indicates the placements.

The flow conditioner is illustrated in Fig. 3.4. The thin one have a thickness of $l_2 = 10$ mm, whereas the thickness of the thick one is $l_3 = 120$ mm. Both of them has porosity of 60%.
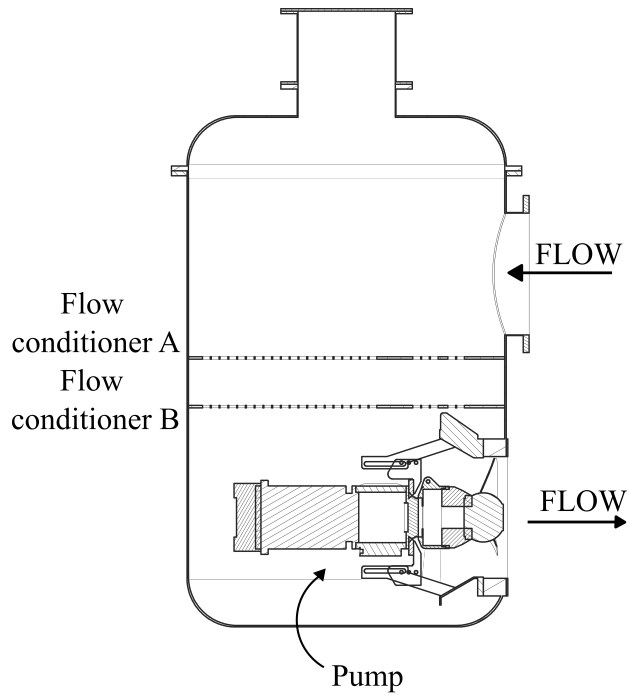
Figure 3.3: Illustration of placements of flow conditioners. Location A and B are the same locations marked in parenthesis in Tab. 3.2.
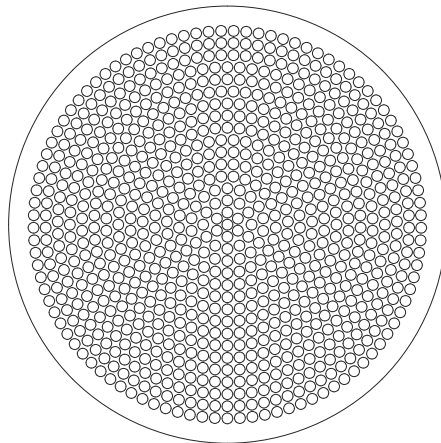
Figure 3.4: Illustration of the flow conditioners placed inside the tank.

3.3   Simplifications

Simplifications in CFD are made to produce higher quality mesh and to cut down on simulation time and memory use. Only simplifications that have minimal effect on the solution or are outside of the scope are made. The biggest geometrical simplifications are connected to the pump housing. This was complex geometry with small details. The original and simplified figures of the pump can be seen in Fig. 3.5. Any small detail present on the main cylinders were removed as well as the placeholders for the shroud. The gaps present between the large cylinders were reduced to simple rectangles and the large cylinders along the central axis were all set to the same diameter.
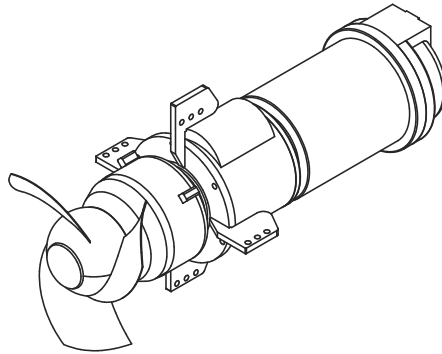
(a) The model provided by the manufacturers.
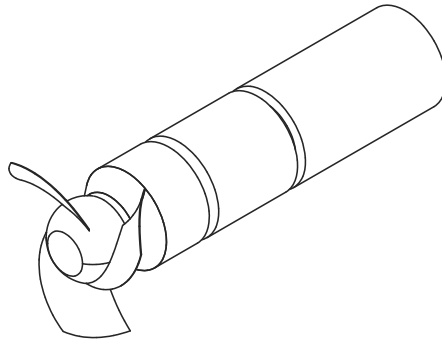
(b) The simplified geometry used in the simulations.

Figure 3.5: The figure is showing a comparison between the original geometry and the simplified one used in the simulations.

There was minimal simplification done to the tank. The filling and drainage pipes were excluded. These would not have affected the flow close to the flow conditioners or the pump. The windows were also removed. This leaves a symmetrical geometry as seen in Fig. 3.6.
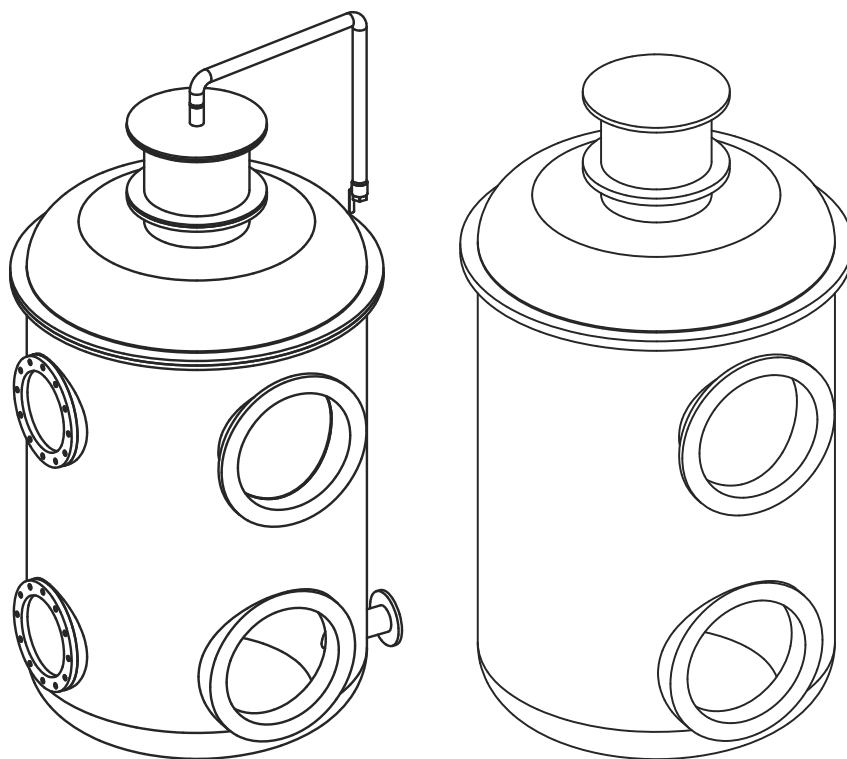
(a) The model provided by the in-house designers.

(b) The simplified geometry used in the simulations.

Figure 3.6: The figure is showing a comparison between the original geometry and the simplified one used in the simulations.

Based on experience from the project thesis it is complicated to create a continues mesh from inside the flow conditioner that connects to the rest of the system. This results an area with low quality mesh where high errors is to expect. An alternative to this is to mesh the parts separately and combining them with an interface. This gets rid of the low-quality mesh area, but introduces error as interpolation between the two sides. It also introduces

another problem. ANSYS® CFX® does not allow for wall boundary conditions to overlap with interfaces, which introduces another source of error. This resulted in the use of a third method; porous domain approach. This method models the flow conditioners as a porous domain. The advantage is that the domain can be meshed as one continues solid and then be assigned the correct porosity at a later stage.

Some simplifications were also made on the blade geometry to improve the mesh quality, reduce the simulation time and reduce the memory needed. This simplification includes round off edges of the blade and removal of the shroud tip clearance. The last change reduces the number of interfaces in simulation by three.

Porous

Porous domain is a domain type in ANSYS® CFX® to model flow through complex geometries such as filters or flow conditioners [32]. A porous domain is a domain with a added momentum sink to the governing equations as seen in Eq. 3.17 - 3.21. The pressure loss coefficient added were found in a combination of literature research and simplified simulation to find an estimated pressure loss. This creates a source of high error when it comes to calculating correct pressure loss through the tank. Due to this error and another aspect explained later in the thesis, the pressure was not considered an important variable to investigate.

Another downside of ANSYS® CFX®'s porous media is that it only allows porous domains to be isotropic. This means the flow can flow in every direction. For the thin flow conditioner, this will have minimal effect. For the thick flow conditioner on the other hand that are designed to straighten the flow, it can cause large errors compared to the physical case. In an attempt to make the porous region anisotropic a directional loss model was used for modeling the pressure loss. The streamwise loss coefficient were the same as the calculated one, whereas the transverse pressure loss coefficient was then set to 100x. This showed to have a positive effect. As seen in Fig. 3.7, the vectors are forced to move in the streamwise direction. On the other hand, this increased the pressure loss a substantial amount. The rest of the settings was left in their default value.
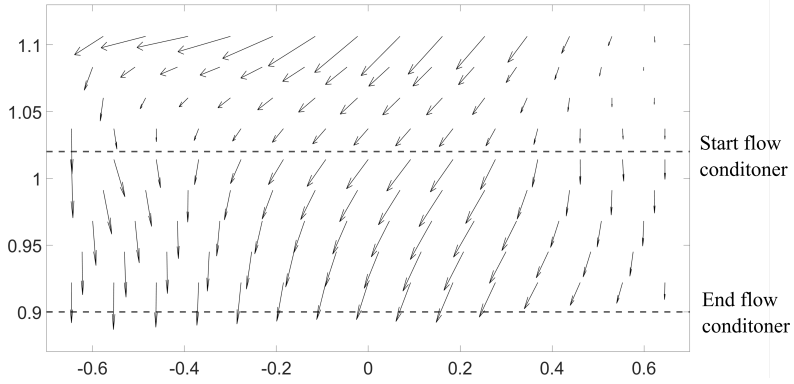
(a) Vector plot when transverse pressure loss is set to 0.
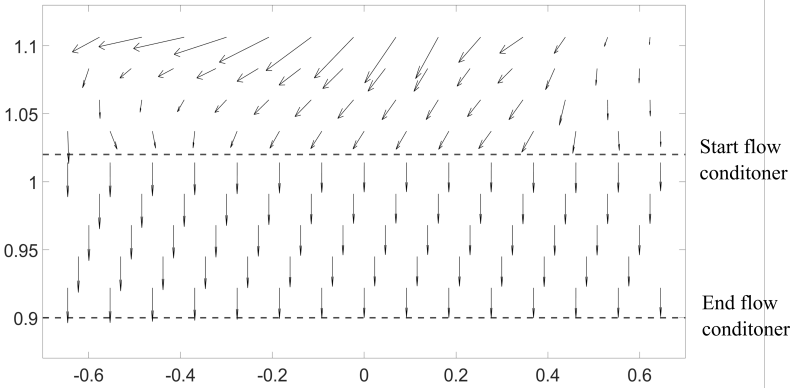
(b) Vector plot when transverse pressure loss is set to 100x more then streamwise direction.

Figure 3.7: Vector field for the thick flow conditioner in configuration 2 when trying to create anisotropic porous media.

3.4   Mesh

The mesh was created by splitting the geometry into smaller subsection and meshing separately. The global settings such as inflation layer was the same for each part, but some local adjustments were made to create a high quality mesh. A completely structured hexahedron mesh was preferred, but some region ended up with unstructured tetrahedron mesh. The number of

element for each part can be seen in Tab. 3.3 alongside some quality aspects.

All the different subsections were connected with an interface that conserves the flux.

Table 3.3: Number of element and some quantifiable meshing qualities.

Part	Number of elements	Average quality	Average y^+	Average orthogonality	Average volume ratio
Inlet pipe	1429120	0.59	110	0.94	1.12
Porous	4640	0.77	7	0.99	1.18
Top of tank	3101087	0.79	84	0.99	1.53
Thin flow conditioner 1	76200	0.75	1.48	0.99	1.09
Mid C1	914400	0.75	7.3	0.99	1.09
Mid C2	419100	0.75	4.6	0.99	1.09
Mid C3	990600	0.75	10.2	0.99	1.09
Mid C4	1066800	0.75	18.3	0.99	1.09
Thin flow conditioner 2	76200	0.75	1.05	0.99	1.09
Thick flow conditioner	571500	0.75	9.7	0.99	1.09
Bot	3518038	0.56	193	0.89	1.27
Pump	5391987	-	42	-	1.21
Outlet	843527	0.37	8	0.99	1.26

Pump

The add-on module turbogrid were used to create the mesh for the pump. Turbogrid automatic creates a mesh by importing a blade, shroud and hub geometry. This was done manually using design modeler. The mesh is easily improved by simple settings. This add on are created for meshing pumps and turbines and creates mesh of high quality. The tip of the pump was not able to be included from design modeler and was therefore included in the outlet pipe as a wall with the same rotational speed as the pump.

3.5 Boundary condition

The boundary conditions used in the simulation were extracted from the pump characteristics given by the manufacturer. A performance curve of the pump was given for rotational speed of 483 min^{-1}, operating mass flow of 1290 m^{3}h[-1] that results in a head of 0.89 m. From the mass flow, the inlet velocity could be calculated to be 4 ms^{-1}. The outlet condition was set as a average static pressure of 0 Pa. The exact absolute pressure in the tank is at

this stage unknown, but an outlet pressure at 0 Pa will provide the pressure distribution in the tank even though the absolute values are incorrect. All the walls were set to smooth, non-slip walls.

The domain created in turbogrid was set as frozen rotor with the rotation speed from the pump characteristic. This means that frame of reference is changed but the relative orientation of the components across the interface is fixed. This reduces the simulation time at the expense of the transient effects. Due to the performance of the pump was outside the scope of this thesis, this was therefore considered an acceptable loss of information.

3.6 Setup

All configuration was simulated transient and initialized by a short steady state simulation. Simulation settings was decided by considering computational time, computer availability, courant number and simulation time. The total time was first set to 5 s based on mass flow and average cross sectional areas. In terms of total tank flow-through it translates to 2. The time step was set to $8\cdot10^{-4}$ s. This number comes from an iterative process finding the best compromise between computational time and courant number. All simulations are run with Menter's SST turbulence model. The most important settings are summarized in Tab. 3.4

Parameter	Setting
Transient scheme	Second Order Backward Euler
Advection scheme	High Resolution
Turbulence numerics	First Order
Inlet velocity	U = 4 ms^{-1}
Outlet pressure	Average static pressure: 0 Pa
Turbulence model	$k - \omega$ SST
Convergence criteria (RMS)	10^{-4}
Convergence control	2
Time step size, Δt	$8\cdot10^{-4}$

Table 3.4: Selected boundary conditions and other parameters for transient simulations.

Eight monitor points are placed around the domain to ensure realistic solution during the simulations.

The simulations ran for approximately 4 days before finishing. After

the simulation completed, a wrongfully boundary condition coupled to the rotational speed of the shroud was discovered, rendering the simulation inaccurate. A continuation simulation was then initialized with the wrongfully simulations and ran for another 2 s for each configuration.

Post processing is done in combination of CFD Post and Matlab to extract the values needed. The planes that were investigated are shown in Fig. 3.8.
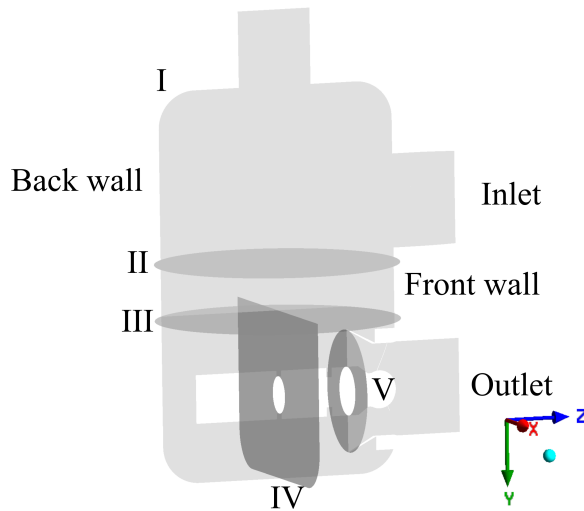
Figure 3.8: Illustration of the main planes where the information presented in the result section is extracted from.

The five planes are chosen to extract the most valuable information. Plane I give overall information on the flow field, can easily recognise regions of recirculation and gives an overall understanding of the flow. Plane II and III are placed before and after the location of the flow conditioners to investigate the effect they have on the flow. Plane IV is placed in the lower half to further investigate the flow field before the pump. The last plane, V, is the inlet to the shroud. The back and front wall is highlighted to simpler describe the results.

3.7 Verification

An important aspect of any CFD simulation is to validate it by comparing it to know experimental values. Normally in this case it is normal to validate against the basis setup and based on that accept the result for the other configurations as realistic solutions. Since this thesis is a part of the design stage of the rig, validation data is not available and these simulations will be validated after the construction of the rig. Instead, the temporary validation is based on recognizing familiar velocity and flow phenomenon behind the flow conditioners based on similar projects as well as performance criteria of the pump given by the manufacturer.

A grid convergence study was conducted in previous work to estimate the discretization errors. Since the geometry is the close to the same, no separate independency test was conducted in this thesis. The element size was adjusted based on the result from that study. The grid convergence index error was found to be 2.52% at the most. The study is reported in the project work [33].

Results and discussions

*The result and discussion chapter present relevant result extracted from the simu-
lations. The results are qualitative results, and uses the transient average values.
The shown results are from the simulations and the configurations defined earlier
in this thesis. Results from tank before the flow conditioners (Plane II) will be
presented first, followed by the region downstream of the flow conditioners (Plane
III, IV and V). Configuration 4 are presented first to establish the basis case and
then the similarities and differences from the other configurations be highlighted.
All the results will be presented before they are discussed.*

As described the the method section, there are a total of four configura-
tions that are investigated, included a base case with no added flow condi-
tioner. The simulation geometry is reduced for the entire system down to
only the tank and an inlet and outlet pipe. The first configuration consists
of two thin flow conditioners at the middle of the tank, the second one was
one thin and one thick flow conditioner. The third one only had one thin
flow conditioner. The rest of the geometry and boundary conditions was
identical for all the simulations. The simulations have all simulated $t = 7$ s,
with values extracted from the last 2 s. Configuration 2 was inserted into
the entire system for one final simulation.

4.1 Analysis of pressurized tank

Figure 4.1 show the streamlines from the inlet pipe entering the tank. The
test section is not included in this figure due to that all configurations show
similar streamlines. The streamlines are cut off after the section with the flow
conditioners. The streamlines for configuration 4 are shown in Fig. 4.1(d)
and set the basis for how the flow will behave without any disturbances. The

flow enters the inlet and proceed to hit the back wall. From there on, the flow divides into two smaller bulk flows. The larger one turns downwards toward the pump whereas the smaller one is forced upward and creates a large swirls at the top of the tank. Some of the top flow also continue to the front of the tank where it is forced downwards into the lower tank. If the streamlines were extended further down the tank and not cut off, there would be streamlines reappearing from the bottom in the area directly under the inlet, where there in the figure is a lack of streamlines. These are excluded to provide a simpler figure.

(a) Streamlines for configuration 1.   (b) Streamlines for configuration 2.

(c) Streamlines for configuration 3.   (d) Streamlines for configuration 4.
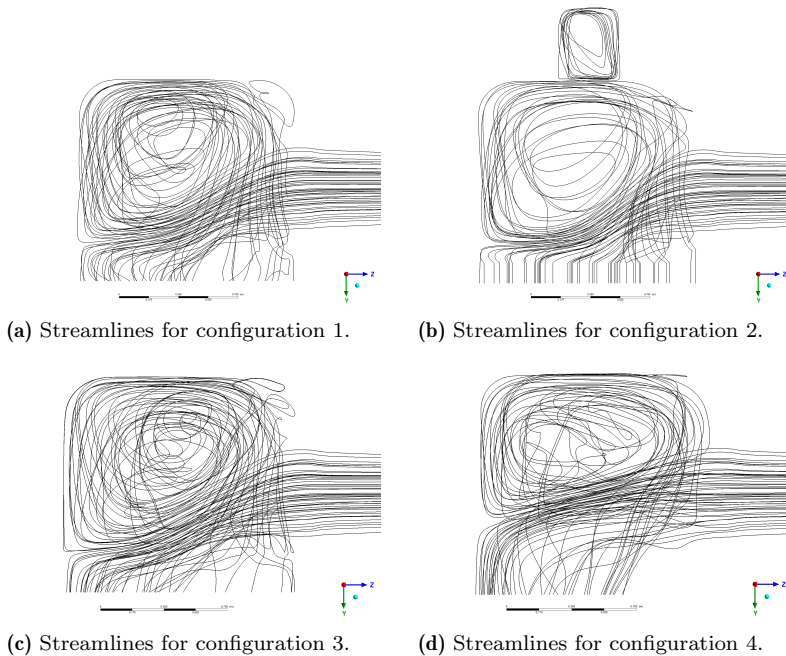
Figure 4.1: Streamlines for all the different configurations. Point of view is from the positive X-direction.

The streamlines in the other configurations have some similarities. When the flow is entering the tank, the flow proceeds to hit the back wall and is consequently divided into two bulk flows. The largest difference compared to configuration 4 is that the flow is forced more downwards by the time it reaches the back wall. This is the case for all the other configurations as well. The result is a larger space at the top for recirculation. Another similarity, that is more distinct for configuration 4, is that most of the flow

30

descend at the back for all the configurations except configuration 2. Here the flow seems more evenly spread.

(a) Transient average velocity V for configurations 1.

(b) Transient average velocity V for configurations 2.

(c) Transient average velocity V for configurations 3.

(d) Transient average velocity V for configurations 4.
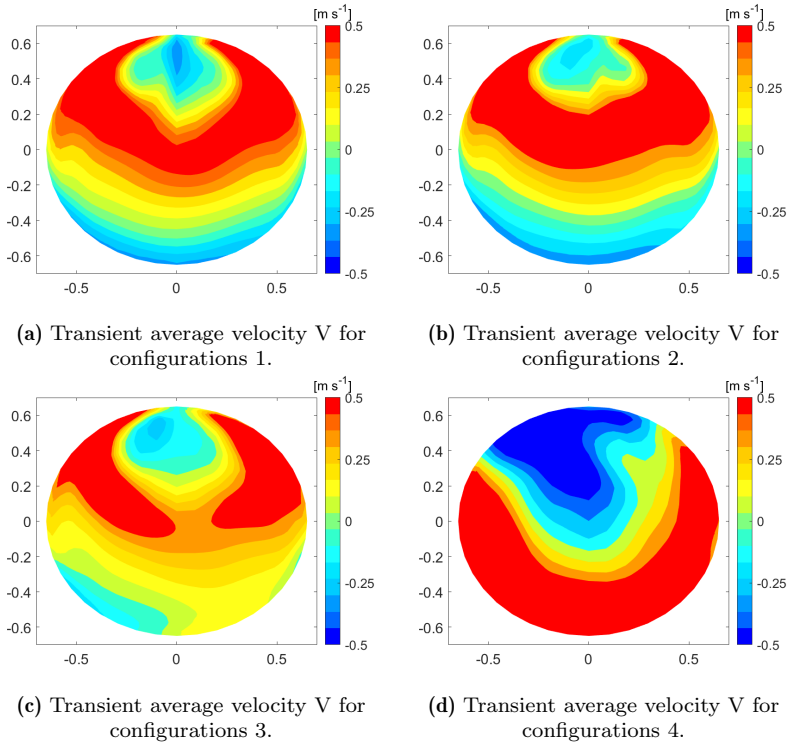
Figure 4.2: Transient average velocity V at plane II for all configurations. y = −0.6 corresponds to the back wall highlighted in Fig. 3.8. Positive values is flow descending in the tank. The point of view is from the negative Y-direction.

The velocity profile in the streamwise direction before the flow conditioners at plane II can be seen in Fig. 4.2. The range is limited to two times the average flow in both positive and negative direction. Configuration 4 has a divided velocity profile. Closer to the back wall and spreading to the sides are a part with high positive velocity magnitudes. At the front wall, there are an area with velocities with the same magnitudes but moving upwards in the tank. The other configurations have a different contour on their velocity profile, but they are quite similar to each other. They can be described as a small region close to the front wall with negative velocity surrounded by a region where there is high positive velocity. The velocity gradually decreases

31

toward the back wall, where the velocity is negative.

The X-component of the vorticity is the only vorticity presented. It is the component with the highest magnitude and is therefore interesting to see the development through the flow conditioners. See Fig. 3.8 to see the coordinate system. The vorticity in the tank is both an indication of velocity gradient, but also gives and indications of areas where circulation occurs. The vorticity that are present at plane II can be seen in Fig. 4.3. For configuration 4, most of the plane is covered by vorticity higher then 5 s^{-1}. There are some areas closer to the side walls there is negative vorticity. The other configurations also have vorticity higher than 5 s^{-1} but in a much more concentrated area in the middle. Closer to the back wall there is an region with negative vorticity.

(a) Transient average X-component of the vorticity for configurations 1.

(b) Transient average X-component of the vorticity for configurations 2.

(c) Transient average X-component of the vorticity for configurations 3.

(d) Transient average X-component of the vorticity for configurations 4.

Figure 4.3: Transient average X-component of the vorticity at plane II for all configurations. y $= -0.6$ corresponds to the back wall highlighted in Fig. 3.8. The point of view is from the negative Y-direction.

To see how the flows is affected by the flow conditioners, Fig. 4.4 show the velocity field in the streamwise direction at plane III. The range is also limited to two times the average velocity. Configuration 4 produces a velocity profile quite similar to plane II. The areas with high positive values have decreased, whereas the negative area has increased. The area between them shows a diffusion of velocity.

(a) Transient average velocity V for configurations 1.

(b) Transient average velocity V for configurations 2.

(c) Transient average velocity V for configurations 3.

(d) Transient average velocity V for configurations 4.
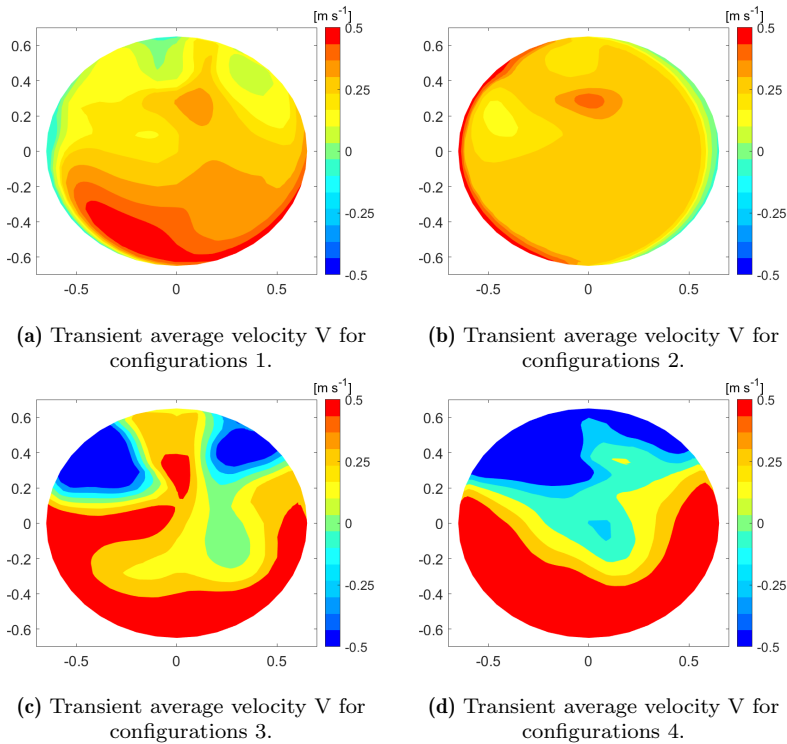
Figure 4.4: Transient average velocity V at plane III for all configurations. $y = -0.6$ corresponds to the back wall highlighted in Fig. 3.8. Positive values is flow descending in the tank. The point of view is from the negative Y-direction.

It is from this plane and onward that makes it clear that the different configurations produce different results. Configuration 1 only have small regions with negative velocities. Most of the values is in the proximity of 0.27 ms^{-1} which is the average velocity. The highest velocity is still close to the back wall. Configuration 2 shows an approximately uniform velocity profile. Only small areas along the walls are deviating. Configuration 3 is

similar to the configuration 4 with the high positive velocity region close to
the back wall and negative at the front wall.

Figure 4.5 shows the X-component of the vorticity at plane III. Con-
figuration 4 shows some variation of values, but most of the plane is still
dominated by mostly positives values. The most extreme values are close
to the back and front wall. Much of the same characteristics can be seen
in configuration 3. One difference is the larger area of negative vorticity at
the top right and left in configuration 3. Configuration 1 and 2 has much
lower values than the two other configurations. Especially configuration 2
that has almost only values very close to zero.

(a) Transient average X-component of the vorticity for configurations 1.

(b) Transient average X-component of the vorticity for configurations 2.

(c) Transient average X-component of the vorticity for configurations 3.

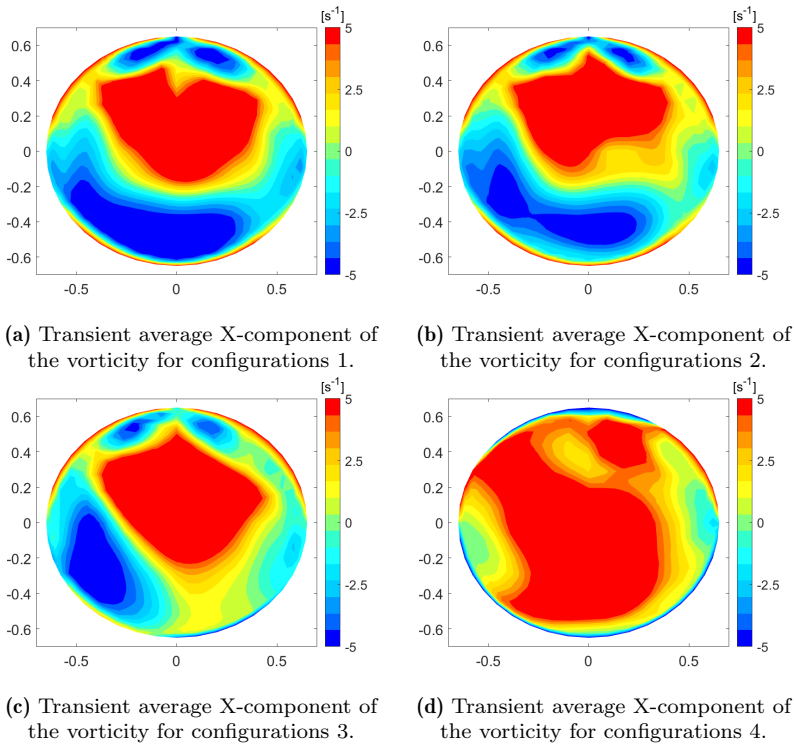**(d)** Transient average X-component of the vorticity for configurations 4.
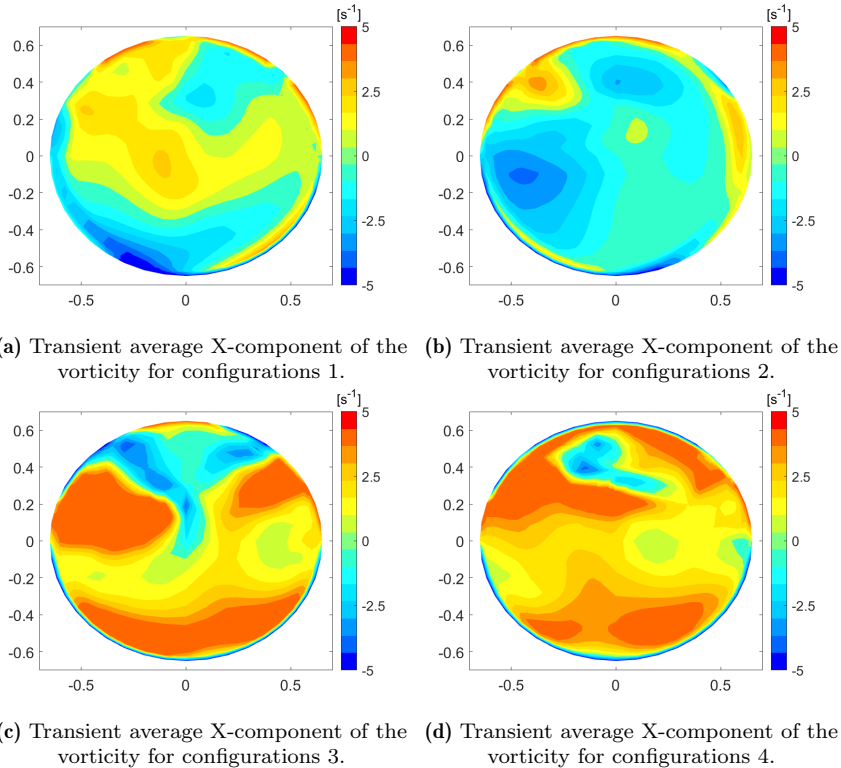
Figure 4.5: Transient average X-component of the vorticity at plane III for all
configurations. y $= -0.6$ corresponds to the back wall highlighted in Fig. 3.8.
The point of view is from the negative Y-direction.

The streamlines for the lower part of the tank from the negative Z-axis

point of view is shown in Fig. 4.6. Configurations 4 characterize as un-structured and random behavior. No clear pattern. The same is true for configuration 3. Configuration 1 and 2 on the other hand show structure in form of one large swirls around the pump body. Another smaller swirl on the left side of the pump body can also be seen. This is easier presented in Fig. 4.7 that shows a vector plot in the lower part of the tank at plane IV.

(a) Streamlines from configuration 1.

(b) Streamlines from configuration 2.

(c) Streamlines from configuration 3.

(d) Streamlines from configuration 4.
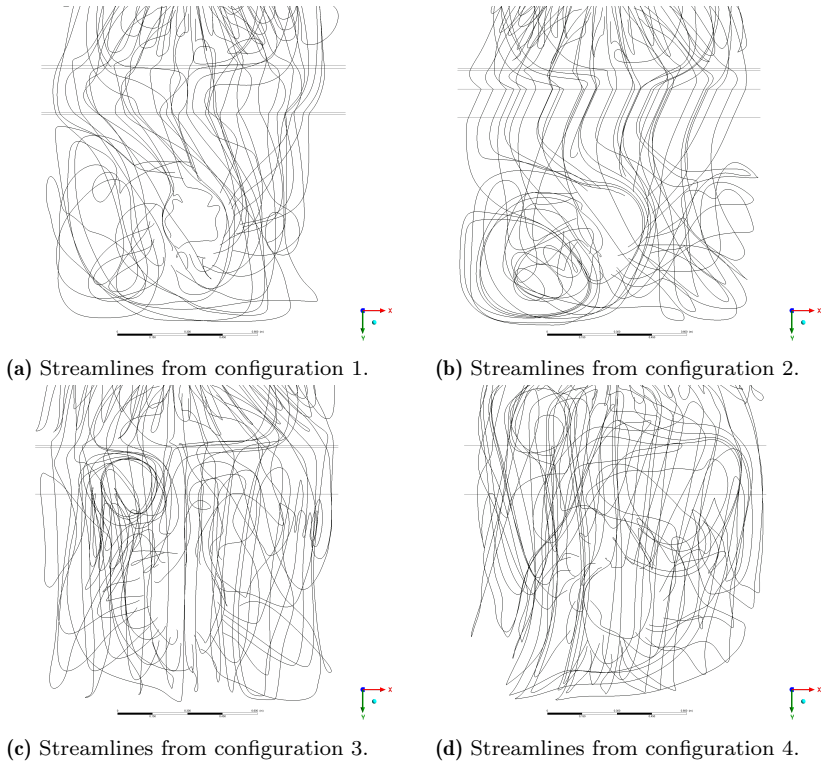
Figure 4.6: Streamlines for all the different configurations for the bot side of the tank at a point of view for the negative Z-direction.

Figure 4.7 makes it clear that configuration 4 has no real structure. The flow is descending from mostly the sides of the cross section. Some flow proceeds to hit the pump body and some flow past it. This flow field results in several swirls and disturbances in the flow. Unstructured flow is also seen in configuration 3. No clear structure is spotted.

Configuration 1 and 2 has one big distinctive swirl in the clockwise di-

rection that define the whole flow. It is in the same direction as the pump rotates. The smaller swirls are located closer to the pump body on the lower left side. The small swirl is at different locations for the two configurations, but the length scale is approximately the same, which is the length scale of the diameter of the pump body. The swirl is at different locations at other planes along the pump body.

(a) Vector plot for configuration 1.

(b) Vector plot for configuration 2.

(c) Vector plot for configuration 3.

(d) Vector plot for configuration 4.
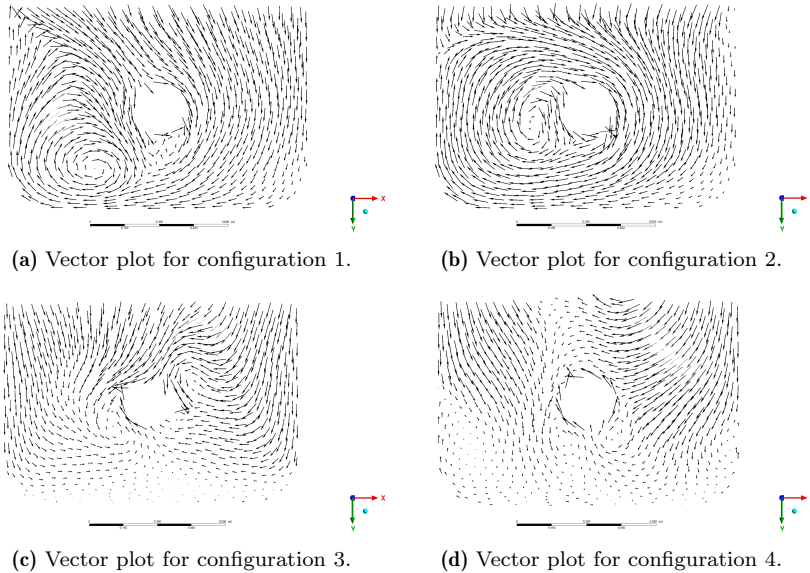
Figure 4.7: Vector plot for plane IV for all of the configuration at a point of view from the negative Z-direction.

Fig 4.8 shows the velocity in the streamwise direction at the shroud inlet, plane V. All the configurations have quite similar velocity profile. Close to the shroud, outer part, there are negative flow. In other words, the flow is returning to the tank. The velocities increase when moving closer to the pump hub. Even though the velocity profile is not uniform over the entire plane, there are symmetry in the theta direction. That means that the velocity is the same for a specific radius. By comparing this velocity profile to profiles further in the shroud, it may indicate that the velocity fields are symmetric in the streamwise direction as well.

The simulated head over the pump is presented in Tab. 4.1. This is one of the only values that can be used for comparing our result to known values.

(a) Transient average velocity W for configuration 1.

(b) Transient average velocity W for configuration 2.

(c) Transient average velocity W for configuration 3.

(d) Transient average velocity W for configuration 4.
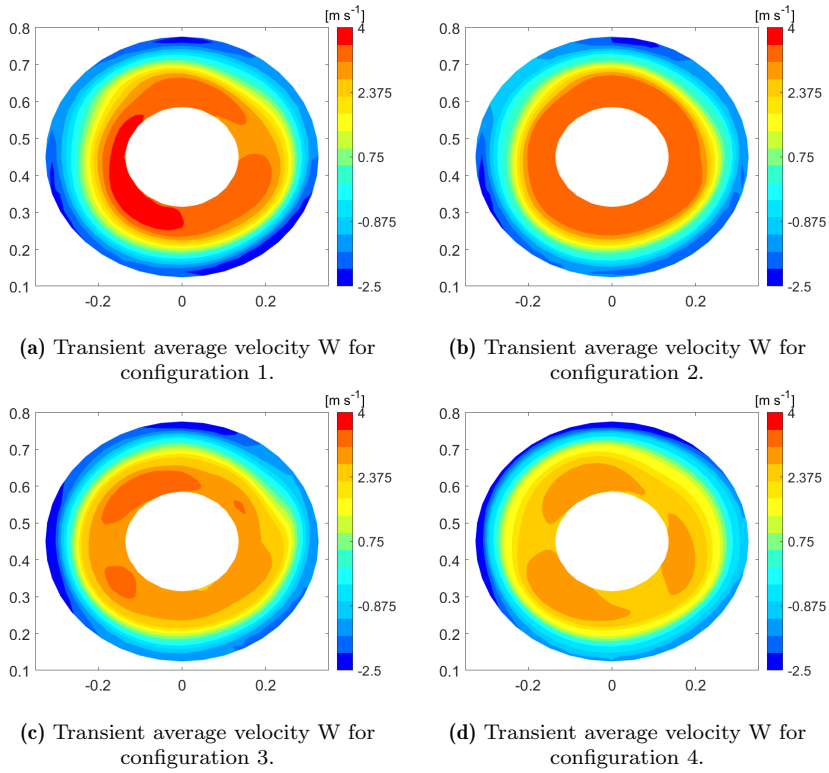
Figure 4.8: Transient average velocity W for all configurations at plane V. This is streamwise direction. The point of view from the negative Z-direction.

The pump is yet to be tested in the configuration, making the head from the pump characteristics the only value to compare to. Pump characteristics are extracted when the pump is running at design condition. This is not necessarily the case for the configurations tested.

There are some variations in the head predicted for the different configurations. Most of the configuration predicts a head that are higher than the one given in pump characteristics. The error is relative and based on the pump characteristics. The error is all within an 10% error of the expected value. The relative error is based on the pump characteristics.

Table 4.1: Head over the pump, calculated at the inlet and outlet of the shroud for the transient average pressure.

Configuration	Head [m]	Error [%]
1	0.97	9.0
2	0.84	-5.6
3	0.92	3.4
4	0.97	9.0
Pump characteristics	0.89	

4.2   Complete water tunnel

Based on the results presented in the previous section, configuration 2 was chosen as the configuration that produced the best quality flow, and was therefore investigated further. A new simulation of the entire experimental rig, including the bends and test section was used. The goal of this simulation was to check if the flow in the tank was affected in the rest of the system and if the entire system was able to create an environment for PIV-measurements in the test section.

(a) Transient average velocity V at plane II.

(b) Transient average velocity V at plane III.
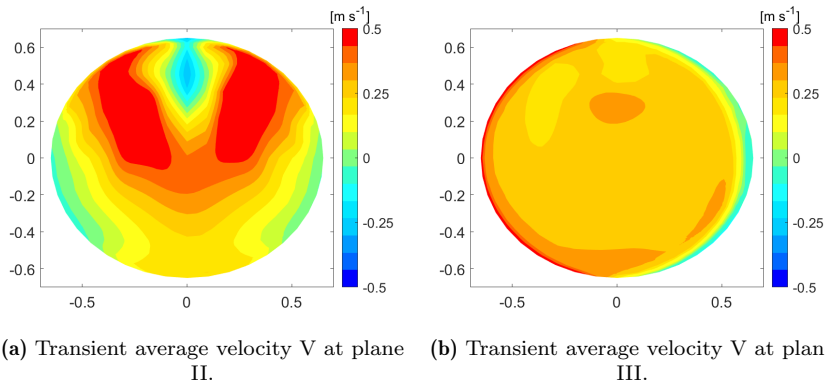
Figure 4.9: Transient average velocity V at plane II and III for configuration 2 expanded to the complete water tunnel. $y = -0.6$ corresponds to the back wall highlighted in Fig. 3.8. The point of view is from the negative Y-direction.

Figure 4.13 shows the velocity field for the entire system. The general flow in the tank is shown as well as how the flow conditioners are working to diffuse the flow and make a calmer velocity field. The most important

aspect of this result is that the flow in the test section is stable and close to uniform that was one of the goals.

Velocity at the same planes was used to compare the simulations. At plane II, the velocity field in the streamwise direction have similar contour as only the tank simulation. The same area with negative velocity close to the front wall are present as well as the area around with high velocity. Closer to the back wall, the flow is still positive, but smaller magnitude. After the flow conditioners, at plane III, the velocity field are close to uniform. Only some areas along the walls with larger deviations. This is close to the profile from the tank only simulation. Both of the velocity fields can be seen in Fig. 4.9.

(a) Transient average vorticity X at plane II.

(b) Transient average vorticity X at plane III.
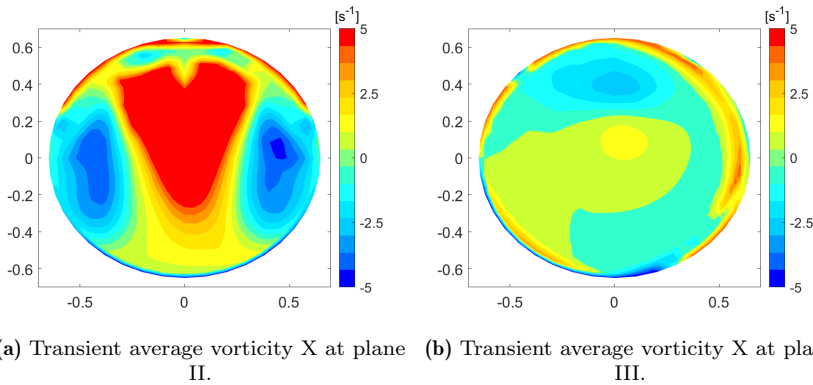
Figure 4.10: Transient average vorticity X at plane II and III for configuration 2 expanded to to the complete water tunnel. y = −0.6 corresponds to the back wall highlighted in Fig. 3.8. The point of view is from the negative Y-direction.

The X component of the vorticity before the tank at plane II shown in Fig. 4.10 be described as close to symmetric. The areas close to the middle is dominated by high positive values, whereas the areas close to the walls are negative. At plane III, most of the vorticity has dissipated and the values are close to zero.

Figure 4.11 shows the velocity vectors at plane IV. The flow is descending from the top with a slight angle and passes the pump body on both sides. When it passes the pump body, it is forced inwards to the middle where it meets. This creates a swirl at the bot right. This swirl is larger in the back of the tank and decreases in size closer to the shroud.

The velocity in streamwise direction for plane V is shown in Fig. 4.12.
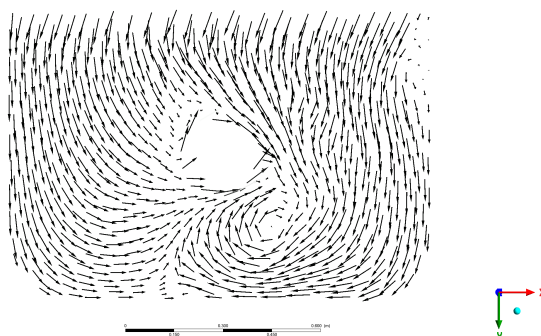
Figure 4.11: Vector plot for plane IV for to the complete water tunnel simulation at a point of view from the negative Z-direction.

The flow close to the hub has large velocity. As the radius increase, the velocity decreases and by the time it has reached the shroud, the magnitude is negative. The velocity field is symmetric for all the different radii.
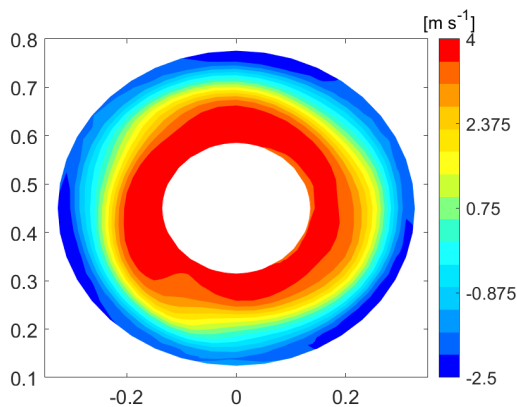
Figure 4.12: Transient average velocity W at plane V for to the complete water tunnel simulation. This is streamwise direction. The point of view from the negative Z-direction.
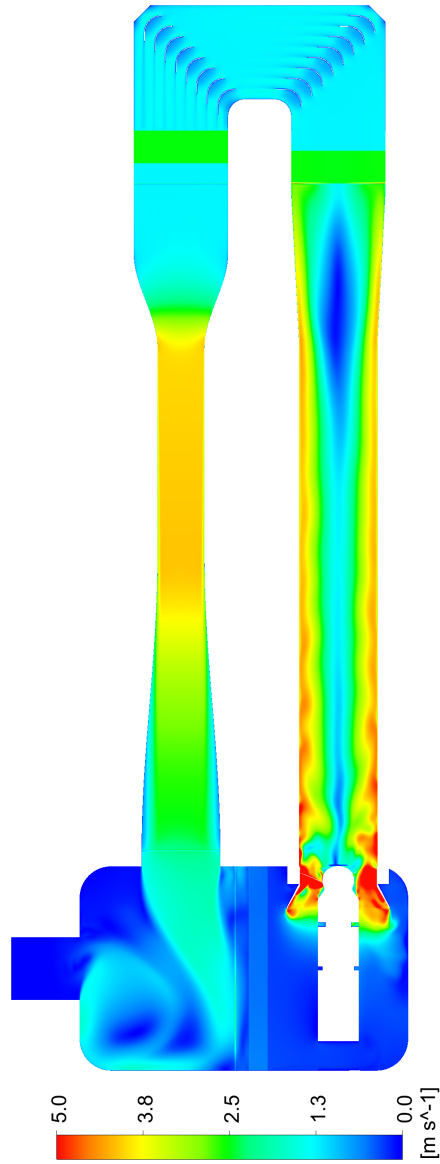
Figure 4.13: Velocity field for to the complete water tunnel simulation.

4.3 Discussion

The large swirl observed at the top of the tank for each configuration is to be expected. It is the same effect covered by the literature [22]. It is one of the effects that creates unsteadiness and that is wanted to be minimized and dissipated by introducing the flow conditioners. As seen in the result, the large swirls at the top is present for all the configuration. Despite some of the configurations creating larges space for swirls, all of the configuration produced a flow field that reminiscent each other. The environment that are created in the top of the tank environment does not affect the flow upstream. This means that the flow in the test section and diffuser will be constant and independent of the configuration in the tank. So from a test section perspective, none of the configurations provide disturbances.

One small effect that the flow conditioners have at the top of the tank is a second recirculating pocket that appears in all of the configuration except configuration 4. The pocket is placed right above the inlet and is a lot smaller then the other swirl. This is similar to the velocity fields found in the literature. This doesn't have large effect, but can be a small source of increased TKE and pressure loss due to the shear layers.

Another effect the flow conditioners have on the top of the tank is making the flow more evenly spread as it descends in the tank. For configuration 4 where the entire cross section is open, the flow stays largely together. This gives one part of the flow a lot of momentum. Flow with large momentum is in itself not a bad thing, but when the goal is to calm and stabilize the flow, a more evenly velocity distribution is desirable. More evenly distributed means less extreme values and as a direct result; fewer extreme effects.

The flow distribution for configuration 1-3 is more evenly. The profiles are however far from uniform or fully developed, so there is room for improvement on the flow in the top tank. Nevertheless, a large improvement from the base case.

When the flow has passed through the flow conditioners, the flow has undergone a large transformation for all the configurations except the basis case. The basis case has nothing interfering with the flow, so the velocity profile development has small changes. The single thin flow conditioner in configuration 3 does not diffuse the large bulk flow on its own. At plane III, most of the flow descend close to the back wall such as configuration 4.

It is at plane III configuration 1 and 2 stands out as the best working configuration. The same tendency as configuration 4 where the flow is pushed

against the back wall is still present in configuration 1, but not as significant. Configuration 2 however ended up with close to uniform flow. The velocity in the other directions are close to zero as well. The thick flow conditioner has clearly the greatest impact on the flow of all the introduced segments.

It is worth to mention that plane III is located much closer to the flow conditioners in configuration 1 and 2. The result of this is that the flow extracted for these two configurations will be a more correct representation of the flow exiting this section whereas for configuration 3 and 4, there are room for the flow in the lower part of the tank to mix and flow freer. It is still of interest to see how the flow behaves at this point for each of the configurations and it gives a clear comparison.

The advantage of the uniform velocity profile is that the flow in a way resets and proceeds to the lower tank with no pre-existing disturbances that can amplify and cause large problems. This does not mean that the flow will be stable and result in a more desirable flow in the lower parts, only that the largest of the disturbances from the inlet does not propagate downstream.

Since both the thin and thick flow conditioners has been modeled as porous media with estimated coefficients for loss and porosity amongst others settings, there are some uncertainties linked to the result. The flow field seen here is therefore not necessarily the true velocity field. However, by looking at the flow, there are indications that the flow field are realistic. The straightening effect seen by the thick flow conditioner is exactly what it is designed for and it is the flow that were expected.

In the lower part of the tank, the flow seemed unstructured, with the exception of configuration 1 and 2. The swirl spotted indicates that the flow in the lower part of the tank is constantly swirling around the pump body. This is a stable flow pattern. A circular swirling motion is also a know phenomenon in the fluid mechanic world, making it possible to predict some flow characteristics. The swirling pattern is also the same flow field that are present inside the pump and in the pipe downstream of the pump. This means that the flow will enter the shroud with correct velocity profile.

The smaller swirl spotted in the lower tank on the other hand can cause greater problem. As stated in the literature research, preexisting vortexes entering the pump can be the source of vibration and instability. If the vortex's length scale of significance when it enters the pump, it could cause a problem. The setup used in this thesis makes it impossible to check if any instability will occur, but it is something to keep in mind.

The inlet flow to the pump looks quite similar in the streamwise direction

for all the configurations. There are however some small swirls at the entry. The first thought would be to assume that these swirls are the same swirls that were seen in configurations 1 and 2, but they are present for configuration 3 and 4 as well, meaning that there are something else that is producing the swirls. Nonetheless, even small swirls can affect the pump performance so there is undesirable that they reach the blades.

The shroud is working as a converger that accelerates the flow. From the literature it is known that vortex filaments stretches when exposed to acceleration. This means that there is a chance for some of these swirls to be stretched out and almost disappear. For configuration 1,3 and 4, the swirls are present when the flow reaches the blade, but in smaller scale. For configuration 2 on the other hand, it seems like the swirls are gone.

A negative aspect that are present in all of the configuration are the backflow at the shroud wall when the flow is entering the pump. This is not a part of the design condition and can highly affect the pump. Flow returning to the tank will also have a opportunity to interfere and disturb the flow in the tank even more.

The errors and variations seen in the pump head can be explained by the swirls and back flow, but can also be explained by some of the simplifications made such as tip gap or frozen rotor. Despite this, the pump is producing a head close to the expected values giving the flow through the pump realistic credibility.

The result extracted for the entire system simulation has some similarities but also some differences from the tank only simulation. At plane II, the velocity fields have the same contour. There are however larger extreme values in the tank only simulation. The area with high velocity has decreased and there is no negative flow at the back wall. For the X-component of the vorticity the values are higher for the entire system simulation before the flow conditioners. Afterward on the other hand the profiles looks similar with values close to zero. Based on these two planes alone it seems like the flow in the tank is calmer when attached to the entire system.

At the lower part of the tank however, the flow is quite different. Instead of having one large clockwise swirl around the pump body, the flow is much more symmetric as it descend into the tank. It creates a swirl similar to the previous simulation, but now it is located on the right side. At different locations alongside the pump body, the swirl is decreasing and by the time the flow reaches the shroud inlet, the swirl is gone. The velocity field in the streamwise direction at plane V is close to identical for the two cases.

—————————Chapter 5—————————

Conclusions

The goal of this thesis was to look at numerous different design configurations for the tank to determine how they affect the flow through the tank and throughout the entire system. The literature reports of large swirls and recirculating pockets occurring for flow entering tanks like the one planned for the experimental rig at the Waterpower Laboratory. Disturbances in the tank can also propagate through the system to the test section. An optimal design can help minimize these swirls, calm the flow and creating a more stable flow field in the water tunnel.

To analyze the configurations, the water tunnel geometry was reduced to the tank with an inlet and outlet pipe. Three configurations with different combinations of flow conditioners were transient simulated with ANSYS® CFX®. The flow conditioners were modeled as porous domains. All configurations were analyzed and compared to each other and a base case where no flow conditioners were omitted. The best performing design was then simulated with the complete water tunnel. The velocity fields, vorticity, and general flow field was used to establish the degree of efficiency for each configuration. Due to the methods used to simplify the flow conditioners, the pressure field was yielded unreliable.

The various configurations produced similar results, but some differences made it possible to determine the superior configuration. In comparison to the base scenario, all three designs had a favorable influence on the flow. They dissipated the flow entering the tank and created a more uniform velocity field through the tank. Vorticity created at the top section of the tank was also reduced by passing the flow conditioners. A recommendation of all the configuration can therefore be made. However, the best producing configuration was configuration 2, with a thin flow conditioner followed by a thick flow conditioner. Downstream of the flow conditioners, this configuration

produced nearly uniform velocity in the streamwise direction, demonstrating its ability to stabilize the flow. It was also the only configuration where no swirls reached the blades in the pump. Configuration 2 provided similar results in the tank for whole water tunnel simulation as well as high-quality flow in the test section.

———————————Chapter 6———————————

Future work

The experimental rig project is still in its start up phase. Several simulation can therefore be carried out to give a deeper understanding of the flow in the water tunnel.

As mentioned earlier, the porous domain approach introduces large errors for the pressure. A way forward would be to remove these simplifications to get a more correct pressure field. Pressure measurements will also be the main method to validate the result when the rig is operational, so correct values can prove valuable.

This thesis has only looked at one operational speed for the pump and flow rate. The rig is planned to have a large operational range. Simulations at different flow rates for configuration 2 could provide confirmation that the tank is stabilizing the flow over the entirety of the operational range.

References

[1] Cattafesta, L., Bahr, C., and Mathew, J., 2010, "Fundamentals of wind-tunnel design," Encyclopedia of aerospace engineering, pp. 1–10, Publisher: John Wiley & Sons.

[2] Valsala, R. R., Son, S. W., Suryan, A., and Kim, H. D., 2019, "Study on reduction in pressure losses in pipe bends using guide vanes," Journal of Visualization, **22**(4), pp. 795–807, Publisher: Springer.

[3] Berga, L., 2016, "The role of hydropower in climate change mitigation and adaptation: a review," Engineering, **2**(3), pp. 313–318, Publisher: Elsevier.

[4] "Hvor kommer strømmen fra? - NVE," accessed 2022-05-26, https://www.nve.no/energi/energisystem/kraftproduksjon/hvor-kommer-strommen-fra/

[5] Barlow, J. B., Rae, W. H., and Pope, A., 1999, *Low-speed wind tunnel testing*, John wiley & sons.

[6] Derbunovich, G. I., Zemskaya, A. S., Repik, E. U., and Sosedko, Y. P., 1987, "Effect of flow contraction on the level of turbulence," Fluid Dynamics, **22**(2), pp. 289–294, Publisher: Springer.

[7] Michalcova, V., Kuznetsov, S., Brozovský, J., and Pospísil, S., 2014, "Numerical and experimental investigations of air flow turbulence characteristics in the wind tunnel contraction," Applied Mechanics and Materials, **617**, pp. 275–279.

[8] Fang, F.-M., Chen, J. C., and Hong, Y. T., 2001, "Experimental and analytical evaluation of flow in a square-to-square wind tunnel contrac-

tion," Journal of wind engineering and industrial aerodynamics, **89**(3), pp. 247–262, Place: Amsterdam Publisher: Elsevier Ltd.

[9] Almeida, O. D., De Miranda, F. C., Neto, O. F., and Saad, F. G., 2018, "Low Subsonic Wind Tunnel – Design and Construction," Journal of Aerospace Technology and Management, **10**, p. 20.

[10] Mehta, R., 1979, "The aerodynamic design of blower tunnels with wide-angle diffusers," Progress in Aerospace Sciences, **18**, pp. 59–120.

[11] Bradshaw, P. and Pankhurst, R. C., 1964, "The design of low-speed wind tunnels," Progress in Aerospace Sciences, **5**, pp. 1–69.

[12] Al-Tameemi, W. T. M. and Ricco, P., "Pressure-loss coefficient of 90∘ sharp-angled mitre elbows," Journal of Fluids Engineering, p. 21.

[13] Han, S. S., Ramamurthy, A. S., and Biron, P. M., 2011, "Characteristics of flow around open channel 90° bends with vanes," Journal of irrigation and drainage engineering, **137**(10), pp. 668–676, Publisher: American Society of Civil Engineers.

[14] Crawford, N. M., Cunningham, G., and Spence, S. W. T., 2007, "An experimental investigation into the pressure drop for turbulent flow in 90° elbow bends," Proceedings of the Institution of Mechanical Engineers, Part E: Journal of Process Mechanical Engineering, **221**(2), pp. 77–88.

[15] International standard, 2003, "NS-EN ISO 5167-1:2003," Norsk Standard, accessed 2022-06-07, https://www.standard.no/no/Nettbutikk/produktkatalogen/Produktpresentasjon/?ProductID=144989

[16] Zhao, T., Zhang, J., and Ma, L., 2011, "A general structural design methodology for multi-hole orifices and its experimental application," Journal of Mechanical Science and Technology, **25**(9), pp. 2237–2246.

[17] Spearman, E. P., Sattary, J. A., and Reader-Harris, M. J., 1996, "Comparison of velocity and turbulence profiles downstream of perforated plate flow conditioners," Flow measurement and Instrumentation, **7**(3-4), pp. 181–199, Publisher: Elsevier.

[18] Erdal, A., 1997, "A numerical investigation of different parameters that affect the performance of a flow conditioner," Flow Measurement and Instrumentation, **8**(2), pp. 93–102.

[19] Chen, R., Tian, M., Chen, S., Tian, W., Su, G., and Qiu, S., 2017, "Three dimensional thermal hydraulic characteristic analysis of reactor core based on porous media method," Annals of Nuclear Energy, **104**, pp. 178–190.

[20] Shi, L., Tang, F., Xie, R., and Zhang, W., 2017, "Numerical and experimental investigation of tank-type axial-flow pump device," Advances in Mechanical Engineering, **9**(3), p. 168781401769568.

[21] Mahgoub, A. O. and Ghani, S., 2021, "Numerical and experimental investigation of utilizing the porous media model for windbreaks CFD simulation," Sustainable Cities and Society, **65**, p. 102648.

[22] Spall, R. E., 1998, "A numerical study of transient mixed convection in cylindrical thermal storage tanks," International Journal of Heat and Mass Transfer, **41**(13), pp. 2003–2011.

[23] Choi, Y.-W., Han, M.-S., Song, J.-H., and Wang, C.-K., 2018, "Analysis of water storage tank flowfield using computational fluid dynamics (CFD) simulation," Journal of Korean Society on Water Environment, **34**(2), pp. 173–182.

[24] Martins, N. M. C. and Covas, D. I. C., 2022, "Induced circulation by plunging and submerged jets in circular water storage tanks using CFD," Water, **14**(8), p. 1277.

[25] American national standard, 2018, "Ansi/HI-9.8," .

[26] Zhang, W., Tang, F., Shi, L., Hu, Q., and Zhou, Y., 2020, "Effects of an inlet vortex on the performance of an axial-flow pump," Energies, **13**(11), p. 2854.

[27] Zhan, J.-m., Wang, B.-c., Yu, L.-h., Li, Y.-s., and Tang, L., 2012, "Numerical investigation of flow patterns in different pump intake systems," Journal of Hydrodynamics, **24**(6), pp. 873–882.

[28] Duan, X., Tang, F., Duan, W., Zhou, W., and Shi, L., 2019, "Experimental investigation on the correlation of pressure pulsation and vibration of axial flow pump," Advances in Mechanical Engineering, **11**(11), p. 168781401988947.

[29] Menter, F. R., 1994, "Two-equation eddy-viscosity turbulence models for engineering applications," AIAA Journal, **32**(8), pp. 1598–1605.

[30] *Ansys meshing User's Guide*.

[31] *CFX-Solver Theory Guide.*

[32] "ANSYS FLUENT 12.0 User's Guide - 7.2.3 Porous Media Conditions," accessed 2022-05-10, https://www.afs.enea.it/project/neptunius/docs/fluent/html/ug/node233.htm

[33] Johnsen, M. D., 2021, "Study of laminar and turbulent flow in controlled environment," M.Sc. thesis/project, Department of Energy and Process Engineering, Norwegian University of Science and Technology, Trondheim, Norway.

—————— Appendices ——————

Appendix A

Master`s Agreement / Main Thesis Agreement

Faculty	Faculty of Engineering
Institute	Department of Energy and Process Engineering
Programme Code	MTPROD
Course Code	TEP4925

Personal Information

Surname, First Name	Johnsen, Magnus Dale
Date of Birth	04.01.1997
Email	magnus.d.johnsen@ntnu.no

Supervision and Co-authors

Supervisor	Chirag Trivedi
Co-supervisors (if applicable)	
Co-authors (if applicable)	

The Master`s thesis

Starting Date	15.01.2022
Submission Deadline	11.06.2022
Thesis Working Title	Study of laminar and turbulent flow in a square cross-section prepared for PIV measurements
Problem Description	Master thesis is continuation of the project work carried out during Autumn 2021. Following research tasks are expected to complete by the candidate during Spring 2022 to qualify for the submission of the master thesis. 1. Continue on numerical modelling of experimental setup with accurate verification and validation. 2. Read literature thoroughly, specifically, boundary layer, large storage tank, flow in bend, diffuser, nozzle, etc. 3. Create high quality numerical model identical to the experimental setup, which is under preparation in the Waterpower Laboratory. 4. Investigate flow field in the experimental loop for different flow conditions, including cavitation, and create performance characteristics considering the entire operating range of the pump. If time available, join laboratory experimentation in the laboratory. 5. Combine all research results and deliver the thesis before the deadline in Spring 2022.

Risk Assessment and Data Management

Will you conduct a Risk Assessment?	Yes
If "Yes", Is the Risk Assessment Conducted?	No
Will you Apply for Data Management? **(REK*, NSD**)**	No
Will You Write a Confidentiality Agreement?	No
If "Yes", Is the Confidentiality Agreement Conducted?	No

* REK -- https://rekportalen.no/

** Norwegian Centre for Research Data (https://nsd.no/nsd/english/index.html)

Topics to be included in the Master`s Degree (if applicable)

—————————— Appendices ——————————

Appendix B

KSB

Project	**Propeller sirk.pumpe**		
Customer pos.no			
Project ID	**4004477355**	Page 1 / 5	
Pos.no	**200**	Created	2021-09-13
Created by	**Angelus, Roland**	Update	2021-11-17

Data sheet

Pump type   **Amaline C 5033-483/64URG**

Operating data

Flow	1.289,7	m³/h	Fluid			
Head	0,9	m	Density		998	kg/m³
Operating speed	483	1/min	Viscosity		1	mm²/s
Shaft power	5,3	kW	Temperature		20	°C
Efficiency	57,8	%	Hydraulic acceptance acc.		ISO 9906 § 4.4.2	
Shut off head	2,2	m				
Inlet chamber	Open inlet chamber					
Minimum water level	1,40	m				

Application range		Head		Flow		Minimum water level	
	From	1,5	m	528,9	m³/h	---	m
	To	0,2	m	2.233,9	m³/h	1,40	m

Design

Design	Submersible pump				
Make	KSB	Impeller type	Axial impeller		
Series	Amaline		Open		
Frame size	500	Degree of propeller		17 °	
Stages	1	Free passage		140	mm
Curve number	K43294/0	Discharge column nominal size		500	mm
Type of bearings	Antifriction	Height of pump			mm
Nos. of bearings	1 / 1	Weight		276	kg
Lubrication	Grease lubrication, lubricated for lifetime				

Materials

Motor casing	Grey cast iron EN-GJL-250 (A 48 Class 35B)
Motor casing cover	Grey cast iron EN-GJL-250 (A 48 Class 35B)
Casing cover	Grey cast iron EN-GJL-250 (A 48 Class 35B)
Gear casing	
Taper piece	Polyurethane
Pump casing	Stainless steel EN-1.4571 (A 276 Type 316 Ti)
Motor shaft	Stainless steel EN-1.4021+QT800 (A 276 Type 420)
Gear unit output shaft	
Propeller	Stainless steel EN-1.4571 (A 276 Type 316 Ti)
Bolts, nuts	Stainless steel A4 (EN-1.4571) (A 276 Type 316)
O-Rings	Viton (FPM)

Project **4004477355**
Customer pos.no
Project ID **Propeller sirk.pumpe**
Pos.no **200**
Created by **Angelus, Roland**

KSB

Page 2 / 5
Created 2021-09-13
Update 2021-11-17

Data sheet

Pump type **Amaline C 5033-483/64URG**

Shaft seal

Cable Entry	Double mechanical seal
Arrangement:	Tandem
Seal on medium side	with elastomer bellows
Mechanical seal, pump-side	Silicon carbide / Silicon carbide
Mechanical seal, bearing-side	Silicon carbide / Silicon carbide

Monitoring

Thermal winding protection	By PTC thermistors
Explosion proof protection	By PTC (Explosion proof models only)
Motor housing monitoring	By conductive moisture sensor electrode
Mechanical seal leakage detection	---
Bearing temperature monitoring	---

Coating

Preparatory treatment	Sa 2 1/2 to ISO 8501-1 / ISO 12 944-4 DIN 55928, Part 4
Blasting method	Steel grit blasting
Primer	Zinc phosphate or Zinc dust
Dry film thickness primer	> 35 microns
Top coat	2-component epoxy resin
Solids content	> 82 %
Dry film thickness top coat	> 150 microns
Colour	Ultramarine Blue (RAL 5002 to DIN 6174)

Project **4004477355**
Customer pos.no
Project ID **Propeller sirk.pumpe**   Page 2.1 / 5
Pos.no **200**   Created   2021-09-13
Created by **Angelus, Roland**   Update   2021-11-17

KSB

Pump type   <u>Amaline C 5033-483/64URG</u>

Installation

INSTALLATION
Type of installation: Horizontal wet-well installation
Connection pipe: DC_DN 500
Submergence, min.:   950 mm
Minimum water level t1 in appl. Range: 1,40 m
Connection to connection pipe: Bolt-free, by claw on pump casing
Guide rail: square pipe 60x60
Guide rail lenght: 3 m (10 ft)
Lifting device: Lifting clamp

Materials:
Connection pipe: galvanized steel
Guide rail: Stainless steel EN-1.4571 (A 276 Type 316 Ti)
Lifting rope: ---
Lifting clamp: Stainless steel EN-1.4571 (A 276 Type 316 Ti)

Scope of supply:
Amaline C 5033-483/64 URG

Following installation parts are in scope of supply:
Joining pipe DN 500, 1m, galv.steel.
Guide rail 60x60x3 m in 1.4571,
Fastening elements for guide rails 60 x 60 x 3 mm,
without middle support for mounting on the tank wall,
incl. chemical anchors M10x130.

Project	**Propeller sirk.pumpe**	
Customer pos.no		
Project ID	**4004477355**	
Pos.no	**200**	
Created by	**Angelus, Roland**	

KSB

Page 15 / 17

Created 2021-09-13
Update 2021-11-17

Performance curve

Pump type **Amaline C 5033-483/64URG**
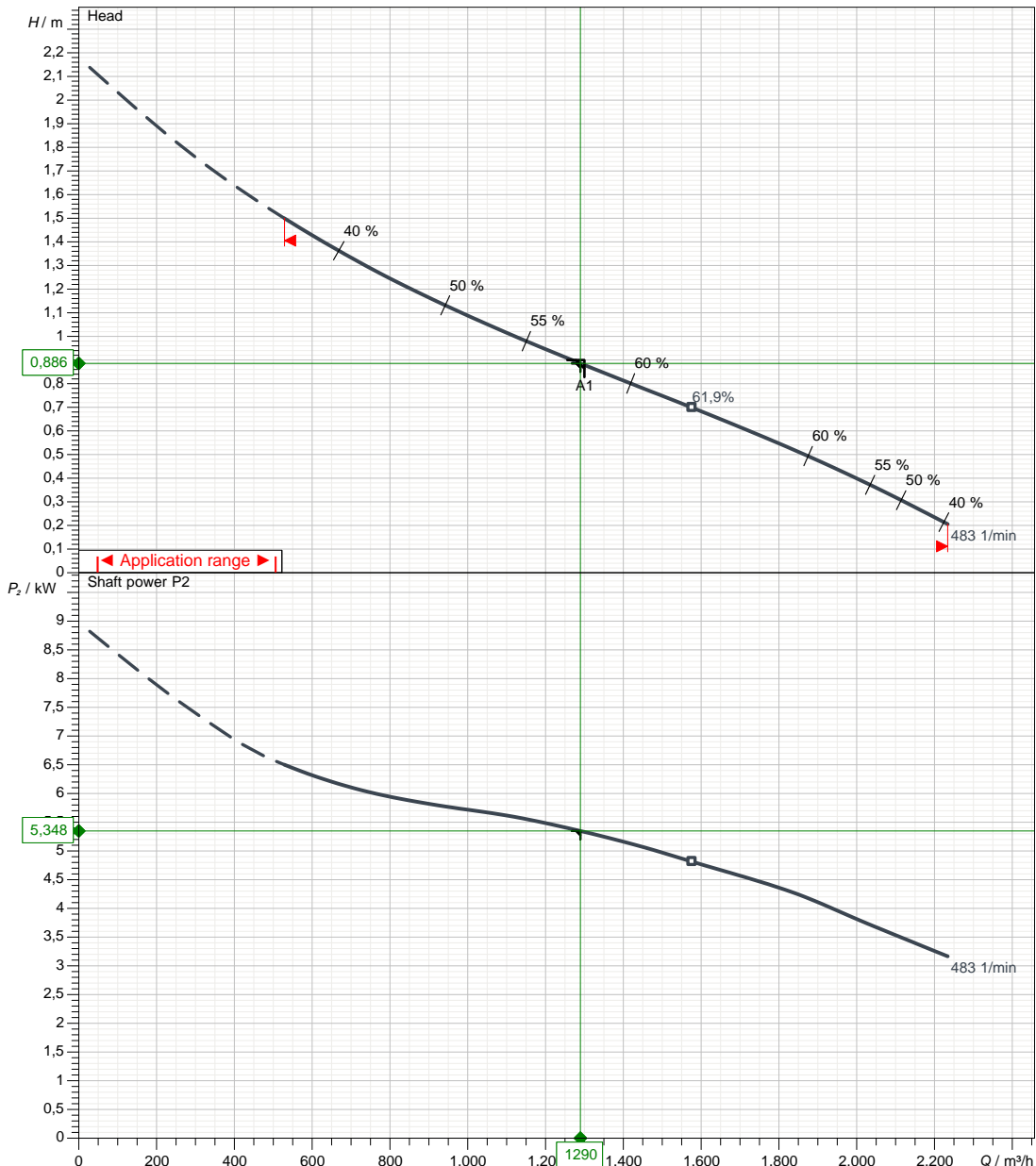
Impeller type	Axial impeller	, Open		Curve number	K43294/0
Free passage	140 mm	Density	998,3 kg/m³	Frequency	50 Hz
Impeller size	485 mm	Viscosity	1,005 mm²/s	Speed	483 1/min

ISO 9906 § 4.4.2

KSB SE & Co. KGaA, Turmstrasse 92, 06110 Halle (Germany), Phone +49 (345) 48260, Fax +49 (345) 4826 4699, www.ksb.com

Frequenz Frequency Fréquence	Baugröße Size Taille	Getriebe Gear unit Engrenage	mm				Gewicht Weight Poids kg
			A	B	Y	X	
50Hz	5033-.../64...	SP189	1376	1235	690	855	276
	5033-.../114...	SP189	1376	1235	690	855	276
	5035-.../64...	SP189	1344	1203	700	865	274,5
60Hz	5035-.../64...	SP189	1376	1235	690	855	276
	5033-.../114...	SP189	1376	1235	690	855	276
	5035-.../114...	SP189	1344	1203	700	865	274,5

Führungsrohr
Guide rail
Pièce de guidage

Anschlussrohr
Connection pipe
Tuyau de raccord

Fließrichtung
Flow direction
Sens d'écoulement

NUR FÜR ANFRAGE/ANGEBOT
technische Änderungen vorbehalten
FOR INQUIRY/OFFER ONLY
technical modifications reserved
SEULEMENT POUR LES DEMANDES/LES OFFRES
sous réserve de modifications technique

Maßstab/Scale/Echelle
1:10
CAD A 2

Aufstellungplan
Installation plan
Plan d'installation

Baureihe-Größe/Type-Size
Amaline P ....-500 G

KSB BE & Co. KGaA
Turmstraße 92-100
D-06110 Halle (Saale)

CAD-BEZEICHNUNG
SCHUTZVERMERK DIN 34

2021/00/02 (Build 213), 32-bit R16.10.03 - 12-10-2021 KSB PU

Project   **Propeller sirk.pumpe**
Customer pos.no
Project ID   **4004477355**   Page 17 / 17
Pos.no   **200**   Created   2021-09-13
Created by   **Angelus, Roland**   Update   2021-11-17

KSB

Data sheet: motor data

Motor type   <u>64URG</u>

Motor manufacturer	KSB SE & Co. KGaA	Rated voltage	400 V
Design acc. standard	IE2	Rated frequency	50 Hz
Degree of protection	IP68	Rated power P2	6,5 kW
Insulation class	F	Rated current	13,1 A
Coolant temperature	< / = 45 °C (113 °F)	Nominal speed	1.475 1/min
Starting mode	Direct starting	Starting to rated current	7,3
No. starts / h	15	Starting current	95,6 A
		Max. voltage	420 V
		Min. voltage	380 V
Motor casing	Grey cast iron EN-GJL-250 (A 48 Class 35B)		
Explosion protection	--		
Pump type	Amaline C 5033-483/64URG		

Load	P1 kW	P2 kW	eta %	cos phi	I A
4/4	7,43	6,5	87,5	0,82	13,1
3/4	5,66	4,9	86,2	0,75	10,9
2/4	3,92	3,3	83,0	0,65	8,7
1/4	2,24	1,6	72,5	0,46	7,0

Main cable	1 x S1BN8-F 12G1.5	Diameter	16,60 mm...17,60 mm
Control cable	---	Diameter	
Cable, outer sheath	Waterproof synthetic rubber compound		
Cable length	10 m (33 ft)		